Human feeding biomechanics: performance, variation, and functional constraints

Justin A. Ledogar, Paul C. Dechow, Qian Wang, Poorva Gharpure, Adam D. Gordon, Karen L. Baab, Amanda L. Smith, Gerhard W. Weber, Ian R. Grosse, Callum F. Ross, Brian G. Richmond, Barth W. Wright, Craig Byron, Stephen Wroe, David S. Strait

The evolution of the modern human (*Homo sapiens*) cranium is characterized by a reduction in the size of the feeding system, including reductions in the size of the facial skeleton, postcanine teeth, and the muscles involved in biting and chewing. The conventional view hypothesizes that gracilization of the human feeding system is related to a shift toward eating foods that were less mechanically challenging to consume and/or foods that were processed using tools before being ingested. This hypothesis predicts that human feeding systems should not produce bite force efficiently and that the cranium should be structurally weak. An alternate hypothesis states that the modern human face is well-configured to generate and withstand high biting forces. We used finite element analysis (FEA) to test these two opposing mechanical hypotheses: that compared to our closest living relative, chimpanzees (*Pan troglodytes*), the modern human craniofacial skeleton is 1) less well configured, or 2) better configured to generate and withstand high magnitude bite forces. We considered intraspecific variation in our examination of human feeding biomechanics by examining a sample of geographically diverse crania that differed notably in shape. We found that our biomechanical models of human crania were, on average, less structurally stiff than the crania of chimpanzees during unilateral biting when loaded with physiologically-scaled muscle loads. Our results also show that modern humans are efficient producers of bite force, consistent with previous analyses. However, highly tensile reaction forces were generated at the working (biting) side jaw joint during unilateral molar bites in which the chewing muscles were recruited with bilateral symmetry. In life, such a configuration would have increased the risk of joint dislocation and constrained the maximum recruitment levels of the masticatory muscles on the balancing (non-biting) side of the head. Our results do not necessarily conflict with the hypothesis that anterior tooth (incisors, canines, premolars) biting could have been selectively important in humans, although the reduced size of the premolars in humans has been shown to increase the risk of tooth crown fracture. We interpret our results, which are not invalidated by large levels of shape-related mechanical variation in strain magnitude or bite force production, to suggest that human craniofacial evolution was probably not driven by selection for high magnitude unilateral biting, and that increased

masticatory muscle efficiency in humans is likely to be a secondary byproduct of selection for some non-dietary function. These results are consistent with the hypothesis that a shift to softer foods and/or the innovation of pre-oral food processing techniques relaxed selective pressures maintaining craniofacial features favoring forceful biting and chewing behaviors, leading to the characteristically small and gracile faces of modern humans.

Human feeding biomechanics: performance, variation, and functional constraints

Justin A. Ledogar[1,2], Paul C. Dechow[3], Qian Wang[3], Poorva Gharpure[3], Adam D. Gordon[1], Karen L. Baab[4], Amanda L. Smith[2,5], Gerhard W. Weber[6], Ian R. Grosse[7], Callum F. Ross[8], Brian G. Richmond[9,10], Barth W. Wright[11], Craig Byron[12], Stephen Wroe[2], David S. Strait[2,5]

[1]Zoology Division, School of Environmental and Rural Science, University of New England, Armidale, NSW, Australia
[2]Department of Anthropology, University at Albany, Albany, NY, USA
[3]Department of Biomedical Sciences, Texas A&M University, Baylor College of Dentistry, Dallas, TX, USA
[4]Department of Anatomy, Midwestern University, Glendale, AZ, USA
[5]Department of Anthropology, Washington University in St. Louis, St. Louis, MO, USA
[6]Department of Anthropology, University of Vienna, Vienna, Austria
[7]Department of Mechanical & Industrial Engineering, University of Massachusetts, Amherst, MA, USA
[8]Department of Organismal Biology & Anatomy, University of Chicago, Chicago, IL, USA
[9]Division of Anthropology, American Museum of Natural History, New York, NY, USA
[10]Department of Human Evolution, Max Planck Institute for Evolutionary Anthropology, Leipzig, Germany
[11]Department of Anatomy, Kansas City University of Medicine and Biosciences, Kansas City, MO, USA
[12]Department of Biology, Mercer University, Macon, GA, USA

Corresponding Author:

Justin A. Ledogar[1,2]

Zoology Division, School of Environmental and Rural Science
University of New England
Armidale, NSW 2351
Australia

Email: jledogar@une.edu.au
Phone: +61 2 6773 5896

Keywords: bone strain, loading, evolution, cranium

46

ABSTRACT

The evolution of the modern human (*Homo sapiens*) cranium is characterized by a reduction in the size of the feeding system, including reductions in the size of the facial skeleton, postcanine teeth, and the muscles involved in biting and chewing. The conventional view hypothesizes that gracilization of the human feeding system is related to a shift toward eating foods that were less mechanically challenging to consume and/or foods that were processed using tools before being ingested. This hypothesis predicts that human feeding systems should not produce bite force efficiently and that the cranium should be structurally weak. An alternate hypothesis states that the modern human face is well-configured to generate and withstand high biting forces. We used finite element analysis (FEA) to test these two opposing mechanical hypotheses: that compared to our closest living relative, chimpanzees (*Pan troglodytes*), the modern human craniofacial skeleton is 1) less well configured, or 2) better configured to generate and withstand high magnitude bite forces. We considered intraspecific variation in our examination of human feeding biomechanics by examining a sample of geographically diverse crania that differed notably in shape. We found that our biomechanical models of human crania were, on average, less structurally stiff than the crania of chimpanzees during unilateral biting when loaded with physiologically-scaled muscle loads. Our results also show that modern humans are efficient producers of bite force, consistent with previous analyses. However, highly tensile reaction forces were generated at the working (biting) side jaw joint during unilateral molar bites in which the chewing muscles were recruited with bilateral symmetry. In life, such a configuration would have increased the risk of joint dislocation and constrained the maximum recruitment levels of the masticatory muscles on the balancing (non-biting) side of the head. Our results do not necessarily conflict with the hypothesis that anterior tooth (incisors, canines,

premolars) biting could have been selectively important in humans, although the reduced size of the premolars in humans has been shown to increase the risk of tooth crown fracture. We interpret our results, which are not invalidated by large levels of shape-related mechanical variation in strain magnitude or bite force production, to suggest that human craniofacial evolution was probably not driven by selection for high magnitude unilateral biting, and that increased masticatory muscle efficiency in humans is likely to be a secondary byproduct of selection for some non-dietary function. These results are consistent with the hypothesis that a shift to softer foods and/or the innovation of pre-oral food processing techniques relaxed selective pressures maintaining craniofacial features favoring forceful biting and chewing behaviors, leading to the characteristically small and gracile faces of modern humans.

93

94

95 **INTRODUCTION**

96 Human craniofacial architecture is extreme among living primate species. In particular,
97 modern humans (*Homo sapiens*) exhibit a tall braincase and a small and short maxilla which
98 distinguishes them from even our closest living relatives, the chimpanzees and bonobos of genus
99 *Pan* (Fleagle, Gilbert & Baden, 2010). Reductions in the size and prognathism of the face,
100 combined with increases in neurocranial globularity, have also been shown to differentiate
101 modern humans from some extinct members of the genus *Homo* (Lieberman, McBratney &
102 Krovitz, 2002). The genus *Homo* exhibits an even more pronounced reduction in the size and
103 robusticity of the facial skeleton, as well as the postcanine dentition and the muscles involved in
104 chewing (e.g., Robinson, 1954; Rak, 1983; Demes & Creel, 1988) relative to australopiths, an
105 extinct informal group of early hominins from which modern humans are likely to be descended
106 (e.g., Walker, 1991; Wood, 1992; Skelton & McHenry, 1992; Strait, Grine & Moniz, 1997; Strait
107 & Grine, 2004; Kimbel, Rak & Johanson, 2004; Berger et al., 2010). Theories purporting to
108 explain the adaptive significance of masticatory reduction in *Homo* frequently stress the
109 importance of changes in diet, usually involving a shift to foods that require less extensive intra-
110 oral processing (e.g., Robinson, 1954; Rak, 1983; Brace, Smith & Hunt, 1991; Wrangham et al.,
111 1999; Lieberman et al., 2004; Ungar, Grine & Teaford, 2006; Wood, 2009). However, a
112 competing view (Wroe et al.,2010), holds that human crania are adapted to produce and resist
113 high feeding loads, based on their finding that the human feeding apparatus is mechanically
114 efficient, requires less muscle force to generate comparable bite reaction forces, and hence

115 requires a less robust structure. This paper evaluates these two alternatives by comparing feeding
116 biomechanics in modern *H. sapiens* to that of chimpanzees (*Pan troglodytes*).

117 A conventional view of cranial gracilization states that this process was spurred by the
118 development of stone tool technologies (e.g., Ungar, Grine & Teaford, 2006). Tool use reduces
119 food particle size (Lucas, 2004), which could allow less biting force per chew and/or fewer
120 chews per feeding bout (Lucas & Luke, 1984; Agrawal et al., 1997). Under this hypothesis, tool
121 use reduces the selective advantage offered by anatomical features that increase muscle force
122 leverage and/or buttress the face against feeding loads. In additional to tool use, increased
123 reliance on meat eating may have played a role in the initial stages of masticatory reduction in
124 early *Homo* (Lieberman, 2008; Ungar, 2012; Zink & Lieberman, 2016). Further gracilization of
125 the jaws and teeth is hypothesized to have occurred with the advent of cooking, which may have
126 been practiced by *H. erectus* (Wrangham, 2009; Organ et al., 2011), by reducing masticatory
127 stresses (Lieberman et al., 2004; Lucas, 2004) and increasing digestive efficiency (Wrangham et
128 al., 1999; Carmody & Wrangham, 2009; Carmody, Weintraub & Wrangham, 2011; Groopman,
129 Carmody & Wrangham, 2015). If gracilization in *Homo* is a consequence of the removal of
130 selection pressure to maintain and resist high magnitude or repetitive bite forces, then human
131 feeding systems should not produce bite force efficiently and the cranium should be structurally
132 weak (i.e., exhibit high stress and strain when exposed to feeding loads).

133 The hypothesis described above is opposed by an alternative interpretation of human
134 feeding mechanics. The marked facial orthognathism exhibited by recent modern humans
135 increases the mechanical advantage (i.e., leverage) of the muscles responsible for elevating the
136 mandible, allowing humans to generate a given bite force with relatively less muscular effort
137 (Spencer & Demes, 1993; O'Connor, Franciscus & Holton, 2005; Lieberman, 2008, 2011; Wroe

et al., 2010; Eng et al., 2013). Many studies interpret bite force efficiency among primate species as being significant in an adaptive sense (Rak, 1983; Strait et al., 2013; Smith et al., 2015a; Ross & Iriarte-Diaz, 2014), with increases in leverage usually expected among species that rely on foods that require forceful biting in order to be processed (e.g., hard seeds or nuts). Therefore, high biting leverage among humans seemingly contrasts with the hypothesis that the human craniofacial skeleton has experienced relaxed selection for traits that favor forceful biting and chewing behaviors (e.g., Brace, Smith & Hunt, 1991; Lieberman et al., 2004; Ungar, Grine & Teaford, 2006; Wood, 2009). However, Wroe et al. (2010) recently investigated human skull form and feeding biomechanics relative to extant apes and fossil australopiths, and found that the human feeding apparatus was mechanically more efficient at producing bite force. Additionally, they found that the human cranium was not obviously more stressed than 3 of the 5 other species examined when models were scaled to the same surface area and bite force. Consequently, Wroe et al. (2010) conclude that the human skull need not be as robust in order to generate, or sustain, bite reaction forces comparable to those of other hominids, and that powerful biting behaviors may have been selectively important in shaping the modern human cranium, although they note that the position of the human temporomandibular joint (TMJ) relative to the occlusal plane may have restricted the ability to consume foods that require powerful, sustained chewing.

Here, we use finite element analysis (FEA) to test these two opposing mechanical hypotheses: that relative to chimpanzees the modern human craniofacial skeleton is 1) less well configured, or 2) better configured to *generate* and *withstand* high magnitude unilateral bite forces. Moreover, our analysis builds on previous research into human craniofacial function (e.g., Lieberman, 2008; Wroe et al., 2010; Szwedowski, Fialkov & Whyne, 2011; Maloul et al., 2012) by examining masticatory biomechanics within the context of the constrained lever model

(Greaves, 1978; Spencer and Demes, 1993; Spencer, 1998, 1999), which predicts that bite force production in mammals is constrained by the risk of generating distractive (tensile) forces at the working (biting) side TMJ. Under this model, during unilateral biting, reaction forces are produced at the bite point and the working and balancing (non-biting) side TMJs. These three points form a "triangle of support", and the line of action of the resultant vector of the jaw elevator muscle forces must intersect this triangle in order to produce a "stable" bite in which compressive reaction forces are generated at all three points (Fig. 1A). The resultant vector lies in the midsagittal plane when the muscles are recruited with bilateral symmetry and will pass through the triangle of support during bites on the incisors, canines, and premolars. However, molar biting changes the shape of the triangle such that a midline muscle result may lie outside of the triangle of support. If this occurs, a distractive (tensile) force is generated in the working side TMJ that "pulls" the mandibular condyle from the articular eminence (Fig. 1B). In the case of the mammalian jaw, the soft tissues of the TMJ are well suited to resist compressive joint reaction forces in which the mandibular condyle is being "driven" into the cranium, but they are poorly configured to resist distractive joint forces in which the condyle is being "pulled away" from the cranium (Greaves, 1978). Mammals, including humans (Spencer, 1998), avoid this situation by reducing the activity of the chewing muscles on the balancing side during bites on the posterior teeth. This draws the muscle resultant vector toward the working side and back within the triangle, but this adjustment reduced the total muscle force available for biting, thereby reducing peak bite force magnitudes. Thus, although one might expect that a bite on a distal tooth would produce an elevated bite force due to a short load arm, this effect is mitigated by the constraint that the muscle force vector must lie within the triangle of support. A finding that constraints on bite force production were especially strong in humans would be consistent

with the hypothesis that the human cranium is poorly configured to generate high unilateral bite forces, and inconsistent with the opposing hypothesis.

Our prior work has shown that high degrees of intraspecific variation in cranial shape need not necessarily produce a high degree of intraspecific mechanical variation (Smith et al., 2015b), implying that mechanical patterns are conservative and reflect an underlying common geometry that may be overlain by skeletal traits that can vary without dramatically altering the fundamental mechanical framework of the cranium. A caveat, however, is that this study (Smith et al., 2015b) examined only one species, *P. troglodytes*. Thus, it has yet to be established whether or not that pattern is generalizable across primates (or other vertebrates). Accordingly, we consider intraspecific variation in our examination of human feeding biomechanics by examining a sample of geographically diverse crania found to differ notably in shape.

MATERIALS & METHODS

Analysis of human cranial shape variation and selection of specimens for FEA

We analyzed finite element models (FEMs) of six crania lying at the extremes of human variation, as well as one "average" specimen found to conform closely to an average shape. To select specimens, we analyzed shape variation within a sample of modern human (*H. sapiens*) crania using previously collected geometric morphometric (GM) data (Baab et al., 2010). We analyzed 85 landmarks collected from a sample of 88 Holocene human crania housed at the American Museum of Natural History (AMNH) (Tables 1, 2). These included mainly facial landmarks combined with a few that characterize neurocranial shape, corresponding to our focus on facial biomechanics in this study. This sample includes individuals from diverse regions across the globe, and provides a cross-section of populations that differ in cranial robusticity

(Baab et al., 2010). Landmark data from these 88 specimens were converted to shape coordinates by Generalized Procrustes analysis (e.g., Bookstein, 1991; Slice, 2005) and analyzed using principal components analysis (PCA). We found that the first 3 principal components (PCs) described 39% of the shape variation in our sample (Fig. 2). In order to maximize shape-related biomechanical variation in our FEMs, we considered variation from all 88 PCs when selecting specimens to be modeled. We first determined those individuals exhibiting the largest distances from the group centroid, calculated as Euclidean distance using all 88 PCs (Table 3). From among these individuals, we chose the six specimens that exhibited the largest pairwise distances, excluding insufficiently preserved crania, those missing teeth, and those unavailable for loan (Table 4). These six "extreme" modern human crania were included: one male and one female Khoe-San individuals from South Africa (AMNH VL/2463 and AMNH VL/2470, hereafter referred to as "KSAN1" and "KSAN2"); a male from Greifenberg, Austria (AMNH VL/3878, "BERG"); a female from the Malay Archipelago (AMNH 99/7889, "MALP"); a male from the Tigara culture at Point Hope, Alaska (AMNH 99.1/511, "TIGA"); and a male from Ashanti, West Africa (AMNH VL/1602, "WAFR"). An additional specimen, a Native American male from Grand Gulch, Utah (AMNH 99/7365, "GRGL"), was chosen as an "average" representative of human cranial shape based on its close proximity (i.e., small Euclidean distance) to the group centroid and its availability for loan (see Table 3). Note that this individual was incorrectly transcribed as AMNH 99/7333 by Ledogar (2015).

Creation of finite element models from "extreme" and "average" human specimens

Construction of solid models

229 The seven specimens chosen for analysis were CT-scanned at Penn State's Center for
230 Quantitative Imaging (pixel size = 0.16 mm) and the 2D digital image stacks were used to create
231 seven solid meshes for use in FEA (Fig. 3) following the methods outlined by Smith et al., 2015
232 (a,b). The solid meshes were then imported as Nastran (NAS) files into Strand7 (Strand7 Pty
233 Ltd) FEA software. We created two sets of human FEMs that differed in their assigned muscle
234 force and bone properties. One set of FEMs ("ALL-HUM" models) was assigned human
235 properties, whereas chimpanzee properties were applied to the second set ("CHIMPED"
236 models). The ALL-HUM analysis provides the most realistic assessment of human cranial
237 mechanics, but the CHIMPED analysis permits direct comparisons of shape-related mechanical
238 variation between chimpanzee and human crania while controlling for all other variables.
239
240 *Material properties of tissues*
241 Human cortical bone material properties assigned to the ALL-HUM models were
242 collected from various locations across the craniofacial skeletons of two fresh-frozen human
243 cadavers (female, aged 22; male, aged 42) by measuring their resistance to ultrasonic wave
244 propagation (see Supplementary Information). For each location sampled, the elastic (Young's)
245 modulus in the axis of maximum stiffness ($E3$) was averaged between the human donors and
246 used to distribute spatially heterogeneous isotropic material properties throughout the seven
247 human FEMs using a method (Davis et al., 2011) analogous to the diffusion of heat through a
248 highly conductive material. To achieve this, values at each of the sampled locations, which
249 ranged from 17.92 GPa to 25.52 GPa (mean=20.61 GPa, SD=1.92), were converted to
250 temperatures and distributed throughout the cortical volume of the FEM. The elastic modulus of
251 cortical bone was then set to vary with temperature during the subsequent loading analysis, with

any thermally-induced strains removed from the analysis. For Poisson's ratio, models were each assigned the average of the sampled locations ($v23 = 0.293$). The same procedure was used to diffuse chimpanzee material properties to the CHIMPED model variants using data from 14 craniofacial regions (Smith et al., 2015a,b). Both sets of model variants were assigned homogeneous and isotropic mechanical properties (trabecular bone: $E3$=637 MPa, $v23$=0.28; enamel, $E3$=80,000 MPa, $v23$=0.28) following Smith et al. (2015a,b).

Muscle forces and constraints

Jaw adductor muscle forces were applied to both sets of FEMs for the anterior temporalis, superficial masseter, deep masseter, and medial pterygoid under the assumption that the chewing muscles were acting at peak activity levels on both sides of the cranium. These loads allow an estimate of the maximum bite force produced by each individual. In the ALL-HUM variants, muscle forces were applied based on muscle physiological cross-sectional area (PCSA) data reported by van Eijden, Korfagen & Brugman (1997). However, these forces were corrected to account for pennation and differences in gape during fixation using formulae from Taylor & Vinyard (2013). Corrected PCSAs were then used to calculate forces in Newtons (N) such that each cm^2 of muscle was equivalent to 30 N (Murphy, 1998). These forces were applied to the "average" specimen (GRGL), while the six "extreme" variants were applied forces that were either scaled up or down based on differences in model volume to the two-thirds power (Table 5). This muscle force scaling procedure removes the effects of differences in size on stress, strain, and strain energy density (Dumont, Grosse & Slater, 2009; Strait et al., 2010), thus focusing the comparison on the functional consequences of shape alone. The same procedure was used to assign chimpanzee muscle forces to the CHIMPED model variants using PCSA data

on an adult female chimpanzee (Strait et al., 2009; Smith et al., 2015a,b). However, rather than scaling the FEMs around the "average" specimen (GRGL), we scaled the forces applied to the CHIMPED models following the scaling relationships in the Smith et al. (2015b) analysis (see Table 5). For both sets of muscle loadings, plate elements were "zipped" at their nodes to the surface faces of tetrahedron elements representing each muscle's origin. The scaled muscle forces for each set of analyses were applied to the plate elements using Boneload (Grosse et al., 2007) and directed toward their respective insertions on the mandible, with the mandible slightly depressed and the condyles translated onto the articular eminences (Dumont, Piccirillo & Grosse, 2010).

For both sets of biting simulations, each of the seven FEMs was constrained at a single node against translation in all directions at the working-side TMJ, while the balancing-side TMJ was constrained in the superoinferior and anteroposterior directions (Strait et al., 2009; Smith et al., 2015a,b), thus creating an axis of rotation around the TMJs. Each model was subjected to simulations of left premolar (P^3) and left molar (M^2) biting by constraining a node in the center of each tooth, respectively, in the superoinferior direction. These constraints generated strains in the craniofacial skeleton, as well as reaction forces at the TMJs and bite point, upon the application of muscle forces.

Analysis of model output parameters

Following Smith et al (2015a,b), we displayed global strain patterns using strain maps. These maps are analogous to histograms in that they illustrate strain magnitudes at thousands of nodes simultaneously, but have the added advantage of preserving spatial information. In addition, we collected strain data from FEMs at 14 locations across the craniofacial skeleton

(Fig. 4). At each location, we examined several strain metrics from each of the seven FEMs in order to understand patterns of deformation. These included maximum principal strain (tension), minimum principal strain (compression), strain mode (the absolute value of maximum principal strain divided by minimum principal strain), shear strain (maximum principal strain – minimum principal strain), von Mises strain (distortional strain or non-isometric strain), and strain energy density (SED, the strain energy stored at a given point). Additionally, strain mode, the absolute value of maximum principal strain divided by minimum principal strain, was recorded for each location. This measure indicates whether tension or compression is dominant at a given location.

Data on the reaction forces generated at constrained nodes (i.e., the bite point and two TMJs) were recorded in Newtons (N). Reaction forces at the P^3 and M^2 were recorded, while reaction forces at the left and right TMJs were recorded and compared relative to a user-defined "triangle of support" Cartesian coordinate system, with one of three axes perpendicular to a reference plane defined by the constrained nodes at the bite point and two articular eminences (Smith et al., 2015a,b). The efficiency of bite force production at a given bite point in each model was also compared using the mechanical advantage (MA), a measure of masticatory muscle efficiency or leverage, calculated as the ratio of bite force output to muscle force input.

In the evaluation of our mechanical hypothesis, we first inspected data collected from the ALL-HUM models for large levels of intraspecific variation that could potentially invalidate the functional significance of our results. Strain magnitudes and SED at each of the 14 sampled locations were examined for large differences between individuals, in addition to a comparison of coefficients of variation (CVs) at specific locations. Differences in the spatial patterning of strain magnitudes between the ALL-HUM models were also compared using strain maps, in addition to variation in biting efficiency (i.e., MA). Lastly, we also calculated CVs for von Mises

strain and MA in the CHIMPED model variants for direct comparison with the chimpanzee CVs reported by Smith et al. (2015b) using the Fligner-Killeen test for equal CVs.

To analyze relative mechanical performance in our human FEMs, we focused on comparisons between the CHIMPED humans and the previously analyzed FEMs of chimpanzee crania (Smith et al., 2015b). Specifically, we compared the magnitudes of von Mises strain, considered to be a key metric in assessing regional bone strength (Keyak & Rossi, 2000), at the 14 sampled locations, as well as differences in biting efficiency between the species. We tested for significant differences between the two species in these data using the Mann-Whitney *U* test.

In vitro validation of specimen-specific human cranial FEM

Data on *in vitro* bone strain collected during simulated P^3 biting in a cadaveric human head were used to validate the findings of our biomechanical analysis of human feeding. As noted above, two human heads were used to gather data on the properties of craniofacial cortical bone. Before the removal of bone samples, the male specimen was CT-scanned, and strain data from 14 craniofacial locations were collected during a series of *in vitro* loading analyses (see Supplementary Information). Digital images of the specimen were then used to construct an eighth FEM, the *in vitro* loadings were replicated using FEA, and strain data were collected from the FEM at locations corresponding to the 14 gage sites. The *in vitro* and *in silico* (i.e., finite element) strain data were compared in order to establish the degree to which assumptions regarding geometry and material properties introduce error into an FEM, where error is represented by the differences between the *in vitro* (observed) and *in silico* (expected) results, divided by the expected results. These data were also analyzed using ordinary least squares

(OLS) regression. Lastly, the orientations for both maximum and minimum principal strain in FEM were compared to those recorded during the *in vitro* loadings.

RESULTS

In vitro validation of specimen-specific human cranial FEM

Strain magnitudes recorded during *in vitro* P^3 loadings of the human cadaveric specimen and the results of the specimen-specific FEA are listed in Table 6. Comparisons of these data reveal that the specimen-specific FEM generated strains very similar in magnitude to those generated during the *in vitro* loadings. Results of the regression analysis on logged data confirm a close correspondence between *in vitro* and *in silico* results, with significant regressions of 0.85x+0.19 (r^2=0.908, p<0.001) and 0.85x+0.19 (r^2=0.953, p<0.001) for maximum principal strain and minimum principal strain, respectively. However, assumptions regarding geometry and material properties did introduce error into the FEA (see Table 6). Principal strain orientations in the specimen-specific FEA were also found to correspond well with the *in vitro* data. The orientations for both maximum principal strain and minimum principal strain in the FEM at the 14 sampled locations were very similar to those recorded from the 14 gage locations during the *in vitro* analysis (Fig. S3 – Fig. S7).

Shape-related variation in human feeding biomechanics

Variation in strain magnitude and spatial patterning

Box-plots of strain and SED distributions recorded from the ALL-HUM models at the 14 sampled locations during premolar (P^3) and molar (M^2) biting are shown in Fig. 5 (see also Tables S1 and S2). Despite notable differences in facial morphology, comparisons of strain

366 magnitudes reveal strong similarities. For P^3 biting, the highest strain magnitudes were
367 experienced at the working nasal margin (Location 12), although on average higher tensile strain
368 magnitudes were generated at the working and balancing postorbital bars (Locations 4 and 5).
369 During M^2 biting, the working zygomatic root (Location 8) was subjected to the highest strain
370 magnitudes, except that tension was greatest at the balancing postorbital bar. During both bites,
371 low strain magnitudes were generated along the supraorbital torus (Locations 1-3), the balancing
372 zygomatic root (Location 9), balancing infraorbital (Location 11), and the zygomatic bodies
373 (Locations 13 and 14). All FEMs of human crania were found to exhibit this general pattern.
374 Some regions of the face did exhibit large differences among individuals. In particular,
375 the FEMs were found to differ in von Mises strain magnitude by as much as 210% at the nasal
376 margin, which also has the highest CVs for all forms of strain during both P^3 and M^2 biting
377 (Table 7), with the exception of minimum principal strain at the working dorsal orbital (Location
378 2) and balancing infraorbital (Location 11) during P^3 biting, SED at the working dorsal orbital
379 (Location 2) during P^3 biting, and the balancing zygomatic body (Location 14) for both bites.
380 Strain mode was nearly always compressive or tensile at a given location across the seven
381 ALL-HUM models (Fig. 6), with a few exceptions. During premolar biting, only 3 locations
382 varied with respect to strain mode (Locations 1, 10, 11), with only one FEM differing from the
383 other models in each case. These three locations also differed in strain mode during molar biting,
384 with Locations 1 and 10 exhibiting slightly higher levels of variation, in addition to variation in
385 strain mode at Location 4.
386 By comparison with CHIMPED FEMs, humans were found to exhibit lower levels of
387 shape-related variation in von Mises strain magnitude and lower CVs than chimpanzees at the 14
388 sampled locations (Table 8). However, results of the Fligner-Killeen tests reveal that only 3 of

389 the 14 "gage sites" exhibit significant differences in CV values. Specifically, humans were found
390 to exhibit a significantly lower CV at the zygomatic arches during both P^3 and M^2 biting at the
391 working infraorbital during P^3 biting.
392
393 *Variation in the spatial patterning of strain concentrations*
394 Despite some large differences in strain magnitude, the spatial patterning of strain
395 distributions was similar across the ALL-HUM models. The color maps during P^3 biting (Fig. 7)
396 reveal two predominant deformation regimes that are common across the seven FEMs: (1)
397 superior displacement of the anterior maxilla in proximity to the loaded P^3, which creates highly
398 tensile and compressive (hence highly shearing) strains surrounding the root of the nasal margin,
399 compression along the nasal margin, and compression at the working zygomatic root; and (2)
400 frontal bending of the zygomae under the inferiorly directed pulling action of the masticatory
401 muscles, which generates tension at the zygomatic body and near the zygomaticomaxillary
402 junction, particularly at the working-side, and deforms the orbit such that it is tensed along an
403 inferolaterally-oriented axis and compressed along a superolaterally-oriented axis.
404 The color maps of strain patterning during M^2 biting were also generally similar across
405 the ALL-HUM models (Fig. 8). As expected, all models exhibited lower strain magnitudes in the
406 lower maxillary region during molar biting compared to premolar biting, but higher
407 concentrations of compressive strain at the working zygomatic root. Molar biting was also
408 associated with the same type of frontal bending, zygomatic torsion, and orbital deformation that
409 was observed for premolar biting, with relatively large concentrations of strain at the postorbital
410 bars, orbital margins, and medial infraorbital.

411 In their study of biomechanical variation in chimpanzee crania, Smith et al. (2015b)
412 illuminated similarities and differences between individuals in the concentrations of relatively
413 high and low strain concentrations by comparing color maps of principal strain magnitudes with
414 the scales normalized to an average of 10 landmarks (Locations 1-5, 8-12), which they suggest
415 may be particularly informative in comparative analyses of craniofacial function. When viewed
416 in this manner (Fig. 9), the human models more clearly reveal a shared pattern of facial
417 deformation that is predominantly characterized by torsion of the zygoma and resulting orbital
418 deformation under the inferiorly-directed masseteric muscle force.
419
420 *Variation in bite force production and efficiency*
421 The ALL-HUM models exhibit moderate differences in bite force production and
422 efficiency (mechanical advantage, MA) at P^3 and M^2 bite points (Table 9). With respect to bite
423 force production, humans generated premolar bite forces that ranged from 333 to 507 N when
424 loaded with scaled masticatory muscle forces. The MA range for premolar biting was 0.34-0.43
425 with all but one individual (WAFR) occupying a narrower range of 0.39-0.43. Molar bite forces
426 ranged from 496 to 756 N. In terms of leverage, most FEMs exhibited molar MAs of 0.57-0.64,
427 but with the WAFR model again being considerably less efficient (0.53).
428 When compared to the chimpanzee data in Smith et al. (2015a), the CHIMPED human
429 models analyzed here were found to exhibit somewhat lower ranges of variation in biting MA.
430 However, results of the Fligner-Killeen tests reveal no significant differences in CV values
431 between the species at either the P^3 (chimp=8.67, human=5.65; p=0.18) or M^2 (chimp=8.11,
432 human=6.67; p=0.13) bite point.
433

Variation in reaction forces generated at the temporomandibular joints

During premolar biting, all seven of the ALL-HUM models generated strongly compressive reaction forces at both TMJs (see Table 9), similar to the results for chimpanzees (Smith et al., 2015b). However, unlike in chimpanzees, M^2 biting generated distractive (tensile) reaction forces at the working-side TMJ that would have "pulled" the mandibular condyle away from the articular eminence in five of the seven models. In order to remove distractive forces, these models required reductions in the muscle force applied to the balancing-side, which ranged from 5% to 15% (see Table 9). Interestingly, when loaded with chimpanzee muscle forces, all seven of the CHIMPED human models exhibit distractive forces in the working TMJ during M^2 biting, with larger muscle force reductions required to eliminate the distraction (see below).

Biomechanical "performance" of human feeding

Structural stiffness of the human craniofacial skeleton

Analysis of the CHIMPED human FEMs reveals that the human craniofacial skeleton generates von Mises strains that are elevated relative to those experienced by chimpanzees under the same simulated loading regimes (Fig. 10). Several of the sampled locations were found to experience significantly higher magnitudes in humans during both P^3 and M^2 biting following the results of Holm-Bonferroni-corrected Mann-Whitney *U* tests (Table 10). These included the working nasal margin (Location 12), postorbital bars (Locations 4 and 5), working zygomatic root (Location 8), and the working dorsal orbital (Location 2). However, strains at the mid-zygomatic arches in humans were within the range observed for chimpanzees (which are extremely variable). Additionally, human zygomatic bodies were found to be structurally stiff, with significantly lower von Mises strain magnitudes than chimpanzees.

457

458 *Human bite force production and mechanical efficiency*

459 Analysis of our CHIMPED human FEMs reveals that human crania are capable of
460 generating bite forces with higher mechanical efficiency than chimpanzees (Fig. 11). Pairwise
461 comparisons using the Mann-Whitey *U* test demonstrate that these differences are significant at
462 both P^3 (U=1.5, z=-2.73, exact p= 0.003) and M^2 (U=1, z=-2.79, exact p=0.002) bite points.
463 However, unlike chimpanzees, all seven of the CHIMPED human models generated highly
464 distractive (tensile) reaction forces at the working-side TMJ during molar biting. Therefore,
465 molar biting in humans increases the risk of having the muscle resultant vector fall outside the
466 triangle of support. To bring the joint back into compression, a reduction in balancing side
467 muscle force of 15%-30% was required (Table 11).

468

469 **DISCUSSION**

470 ***In vitro* validation**

471 In order to validate the findings of our mechanical analysis, we compared *in vitro* bone
472 strain in a cadaveric human head during simulated P^3 biting to the results of a specimen-specific
473 FEA. We found the results of our specimen-specific FEA corresponded quite well with *in vitro*
474 data. In addition to the notable similarities in strain orientation at the 14 sampled locations,
475 results of the regression analysis reveal that FEA can predict *in vitro* strain magnitudes with a
476 high degree of accuracy (r^2 values >0.9). Similarly, Nagasao et al. (2005) were able to validate a
477 dry bone human cranium with a high degree of accuracy (r^2=0.989). However, these authors only
478 examined 2 gage sites and they simulated biting by applying forces to teeth, thus omitting the
479 impact of muscle loading. Toro-Ibacache et al. (2015) also applied point loads to a cadaveric

480 human head and validated strains at two locations in a specimen-specific FEM, finding broad
481 similarities. A greater number of sites were included in an analysis by Szwedowski, Fialkov &
482 Whyne (2011), who found that their FEM results predicted *in vitro* data with an r^2 of 0.73.
483 Although we found excellent correspondence between *in vitro* and *in silico* results, it is
484 clear that FEA does incorporate error (see Table 6). This error was deceptively large at some
485 "gage sites," particularly in areas of low strain. For example, error for maximum principal strains
486 at the balancing dorsal orbital (Location 3) was 80%, but this represents a difference between
487 experimental and FEA results of only 2.67 microstrain (με). Generally speaking, this is not a
488 meaningful difference in the context of vertebrate feeding biomechanics, where some regions of
489 the cranium can experience strain in the thousands of microstrain. However, some moderately
490 strained areas exhibited high error percentages. In particular, the working infraorbital validated
491 well for minimum principal strain, but error for maximum principal strain was nearly 50%. This
492 discrepancy may be related to the morphology of the bone that forms the thin anterior wall of the
493 maxillary sinus, which is susceptible to large modeling errors (Maloul, Fialkov & Whyne, 2011).
494 It is also possible that simplifications to the thin bones of the nasal cavity in the FEM decreased
495 its validity (see Toro-Ibacache et al., 2015). Nonetheless, based on the overall similarity between
496 the *in vitro* and *in silico* analyses in both strain magnitude and orientation, we present the results
497 of our more complex analyses of feeding biomechanics with confidence.
498
499 **Mechanical performance in humans and chimpanzee**
500 *Craniofacial strength: Is the human face weak?*
501 Our results suggest that the modern human craniofacial skeleton is structurally less
502 strong, in terms of resistance to masticatory stress, than that of chimpanzees. In the human

FEMs, most of the locations we analyzed experienced elevated von Mises strain magnitudes, in particular the working nasal margin, the postorbital bars, the working zygomatic root, and the working dorsal orbital region. Exceptions to this pattern include the zygomatic arches, where strains were bracketed by the range of values seen in chimp FEMs, and the prominence of the zygomatic body (i.e., the "cheek bone"), which is apparently strong in modern humans.

In addition to being one of the most variable regions examined, during unilateral P^3 biting the nasal margin of modern humans experienced von Mises strains that were on average more than 350% greater than chimpanzees. Similarly, previous investigations identify the "root" of the nasal margin to be an area of high stress and strain during masticatory loading (Endo, 1965, 1966; Arbel, Hershkovitz & Gross, 2000; Szwedowski, Fialkov & Whyne, 2011; Maloul et al., 2012). This region is often described as a pillar-like structure (Benninghoff, 1925; Bluntschili, 1926), or section of a frame-like structure (Görke, 1902; Endo, 1965, 1966), that resists mainly compression during anterior tooth biting. The results of our analysis are in general agreement with these findings, except that tension at the nasal margin was also found to be high in magnitude, indicating intense bending and shearing of the lower maxillary region during anterior tooth biting (see Fig. 7 and Fig. 9).

In addition to the nasal margin, the postorbital bars of the human FEMs were also found to experience highly elevated von Mises strain magnitudes compared to chimpanzees. However, adjacent regions, including the zygoma/zygomatic body ("cheek bone") region and zygomatic arch, were found to be similar in strength to the lower end of the chimpanzee range. Mechanical analyses of *Paranthropus boisei* and *Australopithecus africanus* (Smith et al., 2015a) show a similar pattern of relatively low strains in the zygomatic body. Strait et al. (2007) found that by thickening the palate in an FEM of a macaque cranium, palatal strains were reduced while those

near the palatal margins, circumorbital region, and zygomatic arches all experienced elevated strain magnitudes. Based on these findings, it is possible that the masticatory stresses generated by our human models that are not being absorbed by stiffer facial regions, like the cheek bone, are being transferred to weaker areas like the postorbital bar and/or other nearby parts of the face.

Smith et al. (2015a) suggest that the structural strength of the zygomatic body in australopiths could be adaptively significant, offering as one possibility that it serves to reduce strains in the nearby zygomatico-maxillary suture. In pigs, it has been demonstrated that unfused sutures can fail at relatively modest stress levels (e.g., Popowics & Herring, 2007), so some bony facial regions may serve to shield nearby sutures from masticatory stresses rather than bone itself (Wang et al., 2012). Among smaller-faced modern human crania, the zygomatico-maxillary suture may be especially prone to experiencing relatively large masticatory stresses. In our FEMs, the largest strains in this region of the mid-face were generated medial to the zygomatico-maxillary suture. The location of these elevated strain magnitudes corresponds roughly to the location of facial fractures experienced commonly during physical altercations (Ellis, El-Attar & Moos, 1985). Facial fractures are also common at the postorbital bar, as opposed to the zygomatic body or zygomatico-maxillary suture, when the zygomatic body is exposed to traumatic blows (Ellis, 2012; Pollock, 2012). Therefore, it is possible that the strength of the human zygomatic body is related to diverting stress from sutures that might otherwise fail under relatively lower stress magnitudes.

In addition to the zygomatic body (“cheek bone”) region, humans were found to exhibit lower average von Mises strains and markedly lower peak strains than chimpanzees at the mid-zygomatic arch, although human values were bracketed by the range of chimp values. This

549 potentially reflects differences in arch length. Specifically, the size of the temporalis muscle,
550 which is correlated with the area of the infratemporal fossa (Weijs & Hillen, 1984), is
551 significantly reduced in humans compared to that of chimpanzees (Taylor & Vinyard, 2013).
552 Demes & Creel (1988) show that the area of the infratemporal fossa is nearly half that of
553 chimpanzees, meaning that the total length of the zygomatic arch is also reduced. Bone strain
554 analyses demonstrate that the arch is subjected to sagittal bending, as well as torsion along its
555 long axis (e.g., Hylander, Johnson & Picq, 1991; Hylander and Johnson, 1997; Ross, 2001; Ross
556 et al., 2011). Predictions based on beam theory therefore suggest that a decrease in the length of
557 the arch will lessen these bending and torsional moments, whereas a reduction in the height
558 and/or breadth of the arch will weaken it under bending and shear, respectively.
559 Functional interpretations based on the morphology of the zygomatic arch are
560 complicated by the fact that the temporalis fascia has been hypothesized to stabilize it from the
561 inferiorly-directed pulling action of the masseter muscle (Eisenberg & Brodie, 1965). Curtis et
562 al. (2011) tested this hypothesis using FEA and found that models that do not include the
563 temporalis fascia will overestimate strains in the arch and surrounding regions, including the
564 postorbital bar and infraorbital. However, they also found that their models lacking a fascia
565 generated strains more similar in magnitude to those collected during *in vivo* experiments
566 (Hylander, Johnson & Picq, 1991; Hylander and Johnson, 1997; Ross, 2001; Ross et al., 2011).
567 Similarly, previous FEA studies on primate crania that have not included a modeled fascia (e.g.,
568 Ross et al., 2005, 2011; Strait et al., 2005) also find broad agreement with *in vivo* data.
569 Importantly, Curtis et al. (2011) did not actually model the temporalis fascia, rather, they applied
570 external forces along the margin of the attachment of the fascia. These forces have moments
571 around the axis of the TMJs, and some of these forces oppose the actions of the jaw adductors.

572 The temporalis fascia should not actually produce forces that are independent of the temporalis
573 muscle, so based on first principles there is reason to be cautious in accepting their results.
574 Therefore we did not feel that it was necessary to include this structure in our FEMs.

575 Although the brow ridges are not thought to play an important role in masticatory stress
576 resistance (e.g., Picq & Hylander, 1989; Hylander, Johnson & Picq, 1991; Ravosa, 1991a,b;
577 Ravosa et al., 2000) it is interesting to note that our human FEMs experienced higher von Mises
578 strain magnitudes than chimpanzees at all three of the supraorbital sites examined, particularly
579 during premolar biting. Between the human and chimpanzee samples, differences were found to
580 be greatest at the working and balancing dorsal orbitals, not the dorsal interorbital, supporting the
581 idea that the brow ridge cannot be modeled as a bent beam (Picq & Hylander, 1989; see also
582 Chalk et al., 2011). The fact that the smaller brows of humans experienced elevated strain
583 magnitudes during biting could be interpreted as meaning that large brow ridges are an
584 adaptation to resist masticatory loads. However, a wealth of experimental data on humans and
585 non-human primate species have shown (e.g., Hylander, Johnson & Picq, 1991; Ravosa et al.,
586 2000; Szwedowski, Fialkov & Whyne, 2011; Ross et al., 2011; Maloul et al., 2012) that strains
587 along the supraorbital margin are relatively low during biting and chewing, which is supported
588 by the results presented here. Therefore, it is more reasonable to interpret differences in
589 supraorbital morphology between humans and chimpanzees as being related to some non-dietary
590 function, and that the resulting increases in brow ridge strain among humans are experienced as a
591 secondary byproduct. For example, Moss and Young (1966) suggest that a large separation is
592 formed posterior to the orbits when brain size is small, forming a supraorbital ridge. When brain
593 size is large, the frontal bone is more steeply inclined posterior to the orbits, forming a vertical

forehead rather than a large torus. A byproduct of this missing bar of bone above the orbits among modern humans could be that strain magnitudes are mildly elevated in that region.

Our results have not been invalidated by large levels of mechanical variation in humans. We found that humans exhibit generally low levels of shape-related mechanical variation in strain magnitude and bite force production. Additionally, though some regions (e.g., the nasal margin) were found to exhibit large differences in strain magnitude, our human FEMs shared a common pattern of the spatial distribution of relatively high and low strain concentrations. These findings are similar to those of Smith et al. (2015b), who found broad similarities in strain patterning among on a sample of chimpanzee FEMs that differed notably in shape. Similarly, Toro-Ibacache, Zapata Muñoz & O'Higgins (2015) found broad similarities between two notably distinct human cranial FEMs.

Overall, our findings show that the human craniofacial skeleton is weaker than that of chimpanzees when subjected to feeding loads. These findings support the hypothesis that dietary changes involving a shift to softer and/or more processed foods along the modern human lineage has led to masticatory gracilization and reduced structural strength of the bony facial skeleton (e.g., Lieberman et al., 2004). However, in their biomechanical analysis, Wroe et al. (2010) recently found that although the human cranium is less robust, it experiences low peak strains and an even distribution of facial strain magnitudes compared to extant apes and fossil australopith species. Differences between our results and those of Wroe et al. (2010) could reflect differences in the way muscle loads were applied to the models in each analysis and/or the manner in which models were constrained. For example, we applied both normal and tangential tractions over entire muscle areas using Boneload (Grosse et al., 2007), whereas Wroe et al. (2010) loaded their models with muscles modeled as straight pre-tensioned beam elements.

However, we conducted a sensitivity analysis to explore this possibility further (see Supplementary Information) and found that these differences in methodology only resulted in small differences in strain magnitude at most locations across the craniofacial skeleton.

Another possible explanation for the differences between our study and the study by Wroe et al. (2010) relates to the magnitudes of the applied muscle forces. Wroe et al. (2010) subjected their FEMs to three sets of simulated biting on various teeth. In their first simulation of the three, FEMs were assigned a set of species-specific muscle forces (or muscle force estimates) from the literature. In a second simulation, models were scaled to the surface area of their chimpanzee model and re-loaded using chimpanzee muscle forces. Lastly, in the third simulation, models were scaled to the surface area of their chimpanzee model and loaded with muscle loads required to generate an equivalent bite force. Based largely on the results of the third simulation, Wroe et al. (2010) hypothesized that the human facial skeleton may in fact be well-adapted to resist masticatory stresses generated during high magnitude biting. However, as noted above, the third simulation involved loading models with muscle forces required to generate an equivalent bite force, and the high biting leverage offered by the retracted human face meant that these forces were relatively low in their human model. More significantly, mean element von Mises stresses were found to be relatively high in their human FEM during the second simulation, where FEMs were scaled to the same surface area and loaded with equivalent muscle forces. This simulation is therefore the most comparable of their three to the analyses performed here, where muscle forces were scaled by volume to the two-thirds power, which we believe is the best means for removing the effects of size on comparisons of mechanical performance (Dumont, Grosse & Slater, 2009; Strait et al., 2010).

Bite force production and efficiency: are humans suited to produce large biting forces?

When analyzed using human bone and muscle properties (i.e., ALL-HUM models), our human FEMs produced bite forces of 333-507 N at the premolar (P^3) and 496-756 N at the molar (M^2). These results are similar to, but lower than, previous estimates of human bite force production using both 2D and 3D modeling techniques (e.g., Wroe et al., 2010; Eng et al., 2013). For example, using skeletal measurements and data on muscle cross-section, Eng et al. (2013) recently estimated that humans are capable of producing approximately 660-1106 N of M^2 bite force, while Wroe et al. (2010) estimated a maximum unilateral M^2 bite force of 1109-1317 N using FEA. However, our M^2 bite force results are bracketed by bite force transducer data collected from various western populations, which range from approximately 368 N (Sinn, de Assis & Throckmorton, 1996) to around 911 N (Waltimo, Nystram & Kananen 1994), although Inuit have been shown to produce an average of 1277 N in M^2 bite force (Waugh, 1937). Therefore, our results for bite force production lie within and do not exceed the known range of *in vivo* variation exhibited by recent human populations.

Because chimpanzees have absolutely and relatively larger jaw adductor muscles than humans (e.g., Taylor & Vinyard, 2013), it is no surprise that the chimp FEMs were capable of producing more forceful bites than our human FEMs when loaded with species-specific muscle forces (compare data in Table 9 to Smith et al., 2015b, Table 4). However, when loaded with muscle forces scaled to remove differences in size, we found that humans are more *efficient* producers of bite forces, in terms of biting leverage, consistent with the findings of Wroe et al. (2010). Specifically, the mechanical advantage (MA) for P^3 biting in humans ranged 0.39-0.47, compared to 0.32-0.42 in chimpanzees (Smith et al., 2015b), with only two chimps overlapping the human range. Humans were found to exhibit even more elevated leverage during M^2 biting

(0.60-0.71), with only one individual overlapping the chimpanzee range (0.49-0.61). When comparing these data using statistical analysis as a heuristic guide, humans were found to be significantly more efficient at producing bite forces at both mesial and distal bite points. The CHIMPED humans were even found to exhibit a biting efficiency similar to that observed in australopiths (Smith et al., 2015a). In fact, P^3 MA in *P. boisei* (0.40) and *A. africanus* (0.41) were near the lower end observed in humans. The FEM of *A. africanus* also generated M^2 bites with similar efficiency (0.62) to humans, whereas *P. boisei* produced more mechanically efficient (0.75) molar bites (Smith et al., 2015a).

Our data on bite force efficiency in humans support previous findings that have demonstrated the mechanical advantage of modern human bony facial architecture compared to both non-modern humans and non-human primate species (e.g., Spencer & Demes, 1993; O'Connor, Franciscus & Holton, 2005; Lieberman, 2008, 2011; Wroe et al., 2010; Eng et al., 2013). Using estimates of muscle leverage from 2D measurements (Lieberman, 2008, 2011), humans have been shown to achieve high biting leverage through a marked degree of facial retraction (orthognathism), which reorients the muscles of mastication relative to the tooth rows. As noted above, we found that our human FEMs produced bite forces with leverage ratios similar to those observed in *A. africanus* and *P. boisei* (Smith et al., 2015a). However, australopiths achieve high biting leverage through an anterior positioning of the chewing muscles relative to the tooth rows (Rak, 1983; Strait et al., 2009, 2010; Smith et al., 2015a). In humans, the midfacial region lies beneath the anterior cranial fossa (Lieberman, McBratney & Krovitz, 2002; Lieberman et al., 2004; Lieberman, 2008, 2011), which similarly places bite points in a position that offers higher mechanical advantage to the jaw adductors.

Although the human cranium can theoretically produce mechanically efficient bite forces, the production of unilateral molar (M^2) bite force is limited by the risk of temporomandibular joint (TMJ) distraction, as predicted by the constrained lever model (Greaves, 1978; Spencer, 1998, 1999). Specifically, we found that all seven of the CHIMPED human FEMs experienced a highly distractive (tensile) reaction force at the working-side joint during molar biting. These forces have the effect of "pulling" the mandibular condyle from the jaw joint, increasing the risk of joint dislocation (Spencer, 1998, 1999). As noted in the introduction, the soft tissues of the mammalian jaw joint are well suited to resist compressive joint reaction forces, but are poorly configured to resist distractive joint forces that "pull" the mandibular condyle from the cranial base (Greaves, 1978; Spencer, 1998, 1999). In contrast, only one of the six chimpanzee FEMs analyzed by Smith et al. (2015a) generated a tensile force at the working TMJ, and this reaction was only very weakly tensile (12.7 N). Similarly, Smith et al. (2015b) found that their FEMs of *P. boisei* and *A. africanus* lacked working-side distraction and were able to produce "stable" bites on both the premolars and molars, offering these species the ability to produce maximally forceful molar bites with limited risk of causing pain and/or damage to the TMJ capsule.

Interestingly, when loaded with human muscle forces (i.e., ALL-HUM), two of the human FEMs (TIGA and WAFR) were capable of maintaining weakly compressive reaction forces at both TMJs during molar biting. Additionally, balancing side force reductions required to eliminate distraction in the remaining models were proportionately less (5-15%) than when applying chimpanzee forces (15%-30%). Comparisons of the muscle loads applied to the models and their force ratios in the ALL-HUM and CHIMPED models (see Tables 9 and 11) reveal that chimpanzees devote a higher proportion of muscle strength to anteriorly-positioned muscle compartments (superficial masseter and anterior temporalis) compared to more posteriorly-

positioned ones (deep masseter and medial pterygoid). Therefore, it is tempting to suggest that changes in human jaw muscle force ratios may have coincided with the retraction of the lower face during human evolution in order to reduce the risk of TMJ distraction. Likewise, if the repositioning of cranial elements for reasons other than food processing led to an increase in biting efficiency but the generation of working side joint distraction during molar biting, the overall reduction of chewing muscle size in *Homo* could also be viewed as a result of positive selection rather than relaxed selection so as to lessen these distractive forces.

Our findings that humans are limited in their ability to produce forceful unilateral molar bites are supported by data on bite force and muscle activity in humans. Spencer (1995, 1998) tested some predictions of the constrained lever model and found that humans produced bite forces that increased as the bite point moved from the incisors to the first molar. Moving from M^1 to M^3, bite forces were found to decrease as a result of the decreasing balancing force muscle recruitment required to avoid joint distraction. Spencer (1995) also notes that most of the participants (8 of 10) in his analysis reported pain near the working-side TMJ when biting forcefully using the back molars. In addition to this study, Hylander (1977) suggests that specialized anterior tooth biting and increased masticatory muscle leverage may be related to the high incidence of third molar reduction and agenesis among modern Inuit due to the increased risk of distraction when biting on these teeth, although the results of our single pre-historic Arctic FEM (TIGA) provide no support for this hypothesis. Similarly, Spencer (2003) demonstrates that seed predating New World primates with adaptations for increased anterior bite force have relatively small third molar roots.

As discussed above, Wroe et al. (2010) analyzed human feeding biomechanics within a comparative context. One of the principal findings of their analysis, supported by the data

731 presented here, is that humans are capable of generating bite forces with higher mechanical
732 efficiency than chimpanzees. Wroe et al. use this as evidence to argue that human craniofacial
733 evolution may have been influenced by selection for powerful biting behaviors. However, the
734 results of this study showing the comparative weakness of the human cranium combined with the
735 increased risk of jaw joint distraction during molar biting leads us to interpret the increased
736 biting leverage exhibited by humans, particularly among recent populations (Spencer & Demes,
737 1993; O'Connor, Franciscus & Holton, 2005), to be a byproduct of human facial orthognathism,
738 which may have been acquired through selection for some non-dietary function. For example,
739 Lieberman (2008, 2011) suggests that the marked degree of facial retraction exhibited by modern
740 human crania could be related to changes in cranial base flexion. However, Ross (2013) shows
741 that basicranial flexion cannot produce significant facial retraction on its own. Instead, Holton et
742 al. (2010) propose that it is the sutural growth restriction of the facial skeleton, not changes in
743 cranial base flexion, which leads to the marked retraction exhibited by modern human crania.
744 Although the majority of the morphological and mechanical evidence is not consistent
745 with the hypothesis that the human masticatory apparatus has experienced recent selection for
746 high magnitude biting, the results of our analysis cannot reject the hypothesis that, in addition to
747 changes in diet and tool use, increases in muscle force efficiency during human evolution could
748 have led to relaxed selection for large chewing muscle size and reductions in facial size (Wroe et
749 al., 2010) or that humans benefited from increased biting leverage when using submaximal
750 forces by exerting less energy per bite. Our results for premolar biting leverage also do not
751 conflict directly with the hypothesis that anterior tooth biting could have been selectively
752 important in humans. However, the reduced size of the premolar teeth in humans increases the
753 risk of tooth crown fracture (Constantino et al., 2010). Therefore, studies on premolar size and

754 strength are not consistent with the hypothesis that humans are particularly well adapted for
755 forcefully loading their anterior teeth, although such studies have yet to be conducted on incisors
756 or canines, which are the more likely to be used during paramasticatory activities. For example,
757 Hylander (1977) identifies features of the modern Inuit craniofacial skeleton that he argues to be
758 adaptations for powerful biting behaviors using the incisors, although our single pre-historic
759 Arctic FEM (TIGA) was not found to be exceptional in this regard. Additionally, Spencer &
760 Ungar (2000) show that incisor bite force leverage varies in relation to the intensity of incisor
761 tooth use among some Native American populations. Similarly, it is possible that differences in
762 anterior tooth use among "archaic" members of the genus *Homo* are reflected in mechanical
763 differences between the species. In particular, the Neanderthals (*H. neanderthalensis*) exhibit a
764 number of derived characteristics hypothesized to be adaptations for forceful incisor biting (e.g.,
765 Brace, 1962; Smith, 1983; Trinkaus, 1983, 1987; Rak, 1986; Demes, 1987). Notably, Spencer &
766 Demes (1993) show that Neanderthals exhibit high incisor bite force leverage relative to *H.*
767 *heidelbergensis* (but not modern *H. sapiens*). In order to maintain functional use of the posterior
768 dentition (i.e., avoid TMJ distraction), Spencer & Demes (1993) further show that the molar
769 tooth row in Neanderthals was anteriorly shifted, resulting in the characteristic retromolar gap.
770 Data on enamel thickness seemingly contrasts with the hypothesis that humans have
771 experienced relaxed selection for powerful biting behaviors. Specifically, a number of studies
772 find that recent human populations exhibit surprisingly thick molar enamel (e.g., Martin, 1983,
773 1985; Olejniczak et al., 2008; Smith et al., 2006; Vogel et al., 2008), which has been interpreted
774 as a primitive retention. However, notwithstanding disagreements over the significance of
775 enamel thickness (Grine, 2005), Smith et al. (2012) recently show that "thick" molar enamel in
776 humans is primarily the result of small coronal dentine areas. They found that enamel area in

777 humans is reduced, but there was a disproportionately large reduction in dentine to enamel as
778 human teeth were evolving smaller size, resulting in a relatively "thick" enamel cap. Thus, Smith
779 et al. (2012) argue that the dichotomy between thick and thin enamel is an oversimplification.
780
781 **CONCLUSIONS**
782 We examined the biomechanical consequences of human masticatory gracilization and
783 intraspecific variation using FEA. Specifically, we tested the hypothesis that the human face is
784 well configured to *generate* and *withstand* high biting forces relative to chimpanzees. We found
785 that our biomechanical models of human crania were, on average, less structurally stiff than the
786 crania of chimpanzees when loaded with physiologically-scaled muscle loads, consistent with
787 small facial size exhibited by modern humans. We also found that modern humans are efficient
788 producers of bite force, consistent with previous analyses (Spencer & Demes, 1993; O'Connor,
789 Franciscus & Holton, 2005; Lieberman, 2008, 2011; Wroe et al., 2010; Eng et al., 2013), but that
790 highly distractive (tensile) reaction forces are generated at the working (biting) side jaw joint
791 during M^2 biting. In life, such a configuration would have increased the risk of joint dislocation
792 and constrained the maximum recruitment levels of the masticatory muscles. Our results do not
793 conflict directly with the hypothesis that premolar biting could have been selectively important
794 in humans, although the reduced size of these teeth in humans has been shown to increase the
795 risk of tooth crown fracture. We interpret our results to suggest that human craniofacial evolution
796 was probably not driven by selection for high magnitude biting, and that increased masticatory
797 muscle efficiency in humans is likely to be a byproduct of selection for some non-dietary
798 function.

Our results provide support for the hypothesis that a shift to the consumption of less mechanically challenging foods and/or the innovation of extra-oral food processing techniques (e.g., stone tool use, cooking) along the lineage leading to modern *Homo sapiens* relaxed the selective pressures maintaining features favoring forceful biting and chewing behaviors, including large teeth and robust facial skeletons, leading to the characteristically small and gracile faces of modern humans (e.g., Brace, Smith & Hunt, 1991; Wrangham et al., 1999; Lieberman et al., 2004; Ungar et al., 2006a,b; Wood, 2009). To contribute to our further understanding, future studies should aim to identify the ecological changes that may have led to the emergence of human-like feeding biomechanics. Were these changes initiated by changes in climate, tool use, diet, food processing, cooking, resource use, or some combination of these factors? To what extent is cranial gracilization part of a general pattern of skeletal gracilization in humans (Ruff et al, 1993, 2015; Chirchir et al, 2015; Ryan & Shaw, 2015)? These questions will be addressed by gaining further insight into the dietary ecology and feeding adaptations of species near the origins of the modern human lineage, including (e.g., *H. habilis*, *H. erectus*) through work on biomechanics, paleoecology, archaeology, bone chemistry, and dental wear, each of which inform key components necessary to obtaining a more complete understanding of human craniofacial evolution.

ACKNOWLEDGEMENTS

We thank Gisselle Garcia-Pack and Kristen Mable of the AMNH for access to human skeletal collections. We also thank Tim Ryan and Tim Stecko of the Center for Quantitative Imaging at Penn State for assistance in acquiring CT image data of modern human crania.

822 **REFERENCES**

823 Agrawal KR, Lucas PW, Prinz JF, Bruce IC. 1997. Mechanical properties of foods responsible
824 for resisting food breakdown in the human mouth. Arch Oral Biol 42:1-9.
825 Arbel G, Hershkovitz I, Gross MD. 2000. Strain distribution on the skull due to occlusal loading:
826 an anthropological perspective. Homo 51:30-55.
827 Baab KL, Freidline SE, Wang SL, Hanson T. 2010. Relationship of cranial robusticity to cranial
828 form, geography and climate in *Homo sapiens*. Am J Phys Anthropol 141:97-115.
829 Benninghoff A. 1925. Spaltlinien am Knochen, ein method zur ermittlung der architektur platter
830 kochen. Verh Anat Ges 34:189-206.
831 Berger LR, de Ruiter DJ, Churchill SE, Schmid P, Carlson KJ, Dirks PHGM, Kibii JM. 2010.
832 *Australopithecus sediba*: a new species of *Homo*-like australopith from South Africa.
833 Science 328:195-204.
834 Bluntschli H. 1926. Rückwirkung des Kieferapparates auf den Gesamtschadel. Z zahnarztl
835 Orthopäd 18:57-59.
836 Bookstein FL. 1991. Morphometric tools for landmark data: geometry and biology. Cambridge:
837 Cambridge University Press.
838 Brace CL. 1962. Cultural factors in the evolution of the human dentition. In: Montague MFA,
839 editor. Culture and the evolution of man. Oxford: Oxford University Press. p 343-354.
840 Brace C, Smith SL, Hunt KD. 1991. What big teeth you had grandma! Human tooth size, past
841 and present. Advances in Dental Anthropology 33-57.
842 Carmody RN, Wrangham RW. 2009. The energetic significance of cooking. J Hum Evol 57:379-
843 391.
844 Carmody RN, Weintraub GS, Wrangham RW. 2011. Energetic consequences of thermal and

845 nonthermal food processing. . Proc Natl Acad Sci USA 108:19199-19203.
846 Chalk J, Richmond BG, Ross CF, Strait DS, Wright BW, Spencer MA, Wang Q, Dechow PC.
847 2011. A finite element analysis of masticatory stress hypotheses. Am J Phys Anthropol.
848 145:1-10.
849 Chirchir H, Kivell TL, Ruff CB, Hublin J-J, Carlson K, Zipfel B, Richmond BG. 2015. Recent
850 origin of low trabecular bone density in modern humans. Proc Natl Acad Sci USA
851 112:366-371.
852 Constantino PJ, Lee JJ-W, Chai H, Zipfel B, Ziscovici C, Lawn BR, Lucas PW. 2010. Tooth
853 chipping can reveal the diet and bite forces of fossil hominins. Biol Lett 6:826-829.
854 Curtis N, Witzel U, Fitton L, O'Higgins P, Fagan M. 2011. The mechanical significance of the
855 temporal fasciae in *Macaca fascicularis*: an investigation using finite element analysis.
856 Davis JL, Dumont ER, Strait DS, Grosse IR. 2011. An efficient method of modeling
857 material properties using a thermal diffusion analogy: an example based on
858 craniofacial bone. PLoS ONE 6:e17004.
859 Demes B. 1987. Another look at an old face: biomechanics of the neandertal facial skeleton
860 reconsidered. J Hum Evol 16:297-303.
861 Demes B, Creel N. 1988. Bite force, diet, and cranial morphology of fossil hominids. J Hum
862 Evol 17:657-670.
863 Dumont ER, Grosse IR, Slater GJ. 2009. Requirements for comparing the performance of
864 finite element models of biological structures. J Theor Biol 256:96-103.
865 Eisenberg NA, Brodie AG. 1965. Antagonism of temporal fascia to masseteric contraction. Anat
866 Rec 152:185-192.
867 Ellis E, El-Attar A, Moos KF. 1985. An analysis of 2,067 cases of zygomatico-orbital fracture. J

868 Oral Maxillofac Surg 43:417-428.
869 Ellis E. 2012. Chapter 16: Fractures of the zygomatic complex and arch. In: Fonseca RJ, Barber
870 HD, Powers MP, Frost DE, editors. Oral and Maxillofacial Trauma. St. Louis, MO:
871 Saunders. p 354-415.
872 Endo B. 1965. Distribution of stress and strain produced in the human facial skeleton by
873 masticatory force. J Anthropol Soc Nippon 73:123-136.
874 Endo B. 1966. Experimental studies on the mechanical significance of the form of the human
875 facial skeleton. J Faculty of Sci 3:1-106.
876 Eng CM, Lieberman DE, Zink KD, Peters MA. 2013. Bite force and occlusal stress production in
877 hominin evolution. Am J Phys Anthropol 151:544-557.
878 Fleagle JG, Gilbert CC, Baden AL. 2010. Primate cranial diversity. Am J Phys Anthropol
879 142:565-578.
880 Görke O. 1904. Beitrag zur funktionellen gestaltung des schadels bei den anthropomorphen und
881 menschen durch untersuchung mit rontgenstrahlen. Arch Anthrop 1:91-108.
882 Greaves WS. 1978. The jaw lever system in ungulates: a new model. J Zool 184:271-285.
883 Grine FE. 2005. Enamel thickness of deciduous and permanent molars in modern *Homo sapiens*.
884 Am J Phys Anthropol. 126:14-31.
885 Groopman EE, Carmody RN, Wrangham RW. 2015. Cooking increases net energy gain from a
886 lipid-rich food. AM J Phys Anthropol 156:11-18.
887 Grosse IR, Dumont ER, Coletta C, Tolleson A. 2007. Techniques for modeling muscle
888 induced forces in finite element models of skeletal structures. Anat Rec 290A:1069-1088.
889 Holton NE, Franciscus RG, Nieves MA, Marshall SD, Reimer SB, Southard, TE, Keller JC,
890 Maddux SD. 2010. Sutural growth restriction and modern human facial evolution: an

experimental study in a pig model. J Anat 216:48-61.

Hylander WL. 1977. The adaptive significance of Eskimo craniofacial morphology. In: Dahlberg AA, Graber TM, editors. Orofacial growth and development. Chicago, IL: Aldine Publishing Company. p 129-169.

Hylander WL, Johnson KR. 1997. *In vivo* bone strain patterns in the zygomatic arch of macaques and the significance of these patterns for functional interpretations of craniofacial form. Am J Phys Anthropol 102:203-232.

Hylander WL, Johnson KR, Picq PG. 1991. Masticatory-stress hypotheses and the supraorbital region of primates. Am J Phys Anthropol 86:1-36.

Keyak JH, Rossi SA. 2000. Prediction of femoral fracture load using finite element models: an examination of stress- and strain-based failure theories. J Biomech 33:209-214.

Kimbel WH, Rak Y, Johanson DC. 2004. The skull of *Australopithecus afarensis*. New York: Oxford University Press.

Ledogar JA. 2015. Human feeding biomechanics: intraspecific variation and evolution. Ph.D dissertation, University at Albany.

Lieberman DE. 2008. Speculations about the selective basis for modern human craniofacial form. Evol Anthropol 17:55-68.

Lieberman DE. 2011. The evolution of the human head. Cambridge, MA: Belknap Press.

Lieberman DE, McBratney BM, Krovitz GE. 2002. The evolution and development of cranial form in *Homo sapiens*. Proc Natl Acad Sci USA 99:1134-1139.

Lieberman DE, Krovitz G, Devlin M, Yates F, St. Clair M. 2004. Effects of food processing on masticatory strain and craniofacial growth in a retrognathic face. J Hum Evol 46:655-677.

Lucas PW. 2004. Dental function morphology: how teeth work. Cambridge: Cambridge

914 University Press.
915 Lucas PW, Luke DA. 1984. Optimum mouthful for food comminution in human mastication.
916 Arch Oral Biol 29:205-210.
917 Maloul A, Fialkov J, Whyne C. 2011. The impact of voxel size-based inaccuracies on the
918 mechanical behavior of thin bone structures. Ann Biomed Eng 39:1092-1100.
919 Maloul A, Regev E, Whyne CM, Beek M, Fialkov JA. 2012. *In vitro* quantification of strain
920 patterns in the craniofacial skeleton due to masseter and temporalis activities. J Craniofac
921 Surg 23:1529-1534.
922 Martin LB. 1983. Relationships of the later Miocene Hominoidea. Ph.D dissertation,
923 Unversity College London.
924 Martin LB. 1985. Significance of enamel thickness in hominoid evolution. Nature 314:260-263.
925 Moss ML, Young RW. 1960. A functional approach to craniology. Am J Phys Anthropol
926 18:281-292.
927 Mundry R, Fischer J. 1998. Use of statistical programs for nonparametric tests of small samples
928 often leads to incorrect p-values: examples from animal behavior. Anim Behav 56:256-
929 259.
930 Murphy RA. 1998. Skeletal muscle. In: Berne RM, Levy MN, editors. Physiology. St. Louis,
931 MO: Mosby. p 294.
932 Nagasao T, Nakajima T, Kimura A, Kaneko T, Jin H, Tamaki T. 2005. The dynamic role of
933 buttress reconstruction after maxillectomy. Plast Reconstr Surg 115:1138-1349.
934 O'Connor CF, Franciscus RG, Holton NE. 2005. Bite force production capability and efficiency
935 in neandertals and modern humans. Am J Phys Anthropol 127:129-151.
936 Olejniczak AJ, Smith TM, Feeney RN, Macchiarelli R, Mazurier A, Bondioli L, Rosas A, Fortea

J, del la Rasilla M, Garcia-Tabernero A, Radovcic J, Skinner MM, Toussaint M, Hublin J-J. 2008. Dental tissue proportions and enamel thickness in Neandertal and modern human molars. J Hum Evol 55:12-23.

Organ C, Nunn CL, Machanda Z, Wrangham RW. 2011. Phylogenetic rate shifts in feeding time during the evolution of *Homo*. Proc Natl Acad Sci USA 108:14555-14559.

Peterson J, Dechow PC. 2002. Material properties of the inner and outer cortical tables of the human parietal bone. Anat Rec 268:7-15.

Picq PG, Hylander WL. 1989. Endo's stress analysis of the primate skull and the functional significance of the supraorbital region. Am J Phys Anthropol 79:393-398.

Pollock RA. 2012. Craniomaxillofacial buttresses: anatomy and operative repair. New York: Thieme Medical Publishers.

Popowics TE, Herring SW. 2007. Load transmission in the nasofrontal suture of the pig, *Sus scrofa*. J Biomech 40:837–844.

Rak Y. 1983. The australopithecine face. New York: Academic Press.

Rak Y. 1986. The Neanderthal face: a new look at an old face. J Hum Evol 15:151-164.

Ravosa MJ. 1991a. Ontogenetic perspective on mechanical and non-mechanical models of primate circumorbital morphology. Am J Phys Anthropol 85: 95-112.

Ravosa MJ. 1991b. Interspecific perspective on mechanical and nonmechanical models of primate circumorbital morphology. Am J Phys Anthropol 86: 369-396.

Ravosa MJ, Noble VE, Hylander WL, Johnson KR, Kowalski EM. 2000. Masticatory stress, orbital orientation and the evolution of the primate postorbital bar. J Hum Evol 38:667-693.

Robinson JT. 1954. Prehominid dentition and hominid evolution. Evolution (N Y) 8:325-334.

960 Ross CF. 2001. *In vivo* function of the craniofacial haft: the interorbital "pillar." Am J Phys
961 Anthropol 116:108-139.
962 Ross CF. 2013. Complexity, modularity, and integration in the human head. J Hum Evol 64:56-
963 67.
964 Ross CF, Iriarte-Diaz J. 2014. What does feeding system morphology tell us about feeding? Evol
965 Anthropol 23:105-120.
966 Ross CF, Patel BA, Slice DE, Strait DS, Dechow PC, Richmond BG, Spencer MA. 2005.
967 Modeling masticatory muscle force in finite-element analysis: sensitivity analysis using
968 principal coordinates analysis. Ant Rec 283A:288-299.
969 Ross CF, Berthaume MA, Dechow PC, Iriate-Diaz J, Porro LB, Richmond BG, Spencer M,
970 Strait DS. 2011. *In vivo* bone strain and finite-element modeling of the craniofacial haft
971 in catarrhine primates. J Anat 218:112-141.
972 Ruff CB, Trinkaus E, Walker AC, Larsen CS. 1993. Postcranial robusticity in *Homo*. I:
973 Temporal
974 trends and mechanical interpretation. Am J Phys Anthropol. 91: 21-53.
975 Ruff CB, Holt B, Niskanen M, Sladek V, Berner M, Garofalo E, Garvin HM, Hora M, Junno J-
976 A,
977 Schuplerova E, Vilkama R, Whittey E. 2015. Gradual decline in mobility with the
978 adoption of food production in Europe. Proc Natl Acad Sci USA 112:7147-7152.
979 Ryan TM, Shaw CN. 2015. Gracility of the modern *Homo sapiens* skeleton is the result of
980 decreased biomechanical loading. Proc Natl Acad Sci USA 112:372-377.
981 Schwartz-Dabney CL, Dechow PC. 2002. Accuracy of elastic property measurement in
982 mandibular cortical bone is improved by using cylindrical specimens. J Biomech

983 Eng 124:714-723.
984 Sinn DP, de Assis EA, Throckmorton GS. 1996. Mandibular excursions and maximum bite
985 forces in patients with temporomandibular joint disorders. J Oral Maxillofac Surg
986 54:671-679.
987 Skelton RR, McHenry HM. 1992. Evolutionary relationships among early hominids. J Hum Evol
988 23:309-349.
989 Slice DE, ed. 2005. Modern morphometrics in physical anthropology, vol. 6. Springer Science &
990 Business Media.
991 Smith FH. 1983. Behavioral interpretations of changes in craniofacial morphology across the
992 archaic/modern *Homo sapiens* transition. In. Trinkaus E, editor. The Mousterian legacy.
993 BAR. p. 141-163.
994 Smith AL, Benazzi S, Ledogar JA, Tamvada K, Pryor Smith LC, Weber GW, Spencer MA,
995 Lucas PW, Michael S, Shekeban A, Al-Fadhalah K, Almusallam AS, Dechow PC,
996 Groasse IR, Ross CF, Madden RH, Richmond BG, Wright BW, Wang Q, Byron C, Slice
997 DE, Wood S, Dzialo C, Berthaume MA, van Casteren A, Strait DS. 2015a. The feeding
998 biomechanics and dietary ecology of *Paranthropus boisei*. Ant Rec 298:145-167.
999 Smith AL, Benazzi S, Ledogar JA, Tamvada K, Pryor Smith LC, Weber GW, Spencer MA,
1000 Dechow PC, Grosse IR, Ross CF, Richmond BG, Wright BW, Wang Q, Byron C, Slice
1001 DE, Strait DS. 2015b. Biomechanical implications of intraspecific shape variation in
1002 chimpanzee crania: moving towards an integration of geometric morphometrics and finite
1003 element analysis. Anat Rec 298:122-144.
1004 Smith TM, Olejniczak AJ, Reid DJ, Ferrell RJ, Hublin JJ. 2006. Modern human molar enamel
1005 thickness and enamel-dentine junction shape. Arch Oral Biol 51:974-995.

1006 Smith TM, Olejniczak AJ, Zermeno JP, Tafforeau P, Skinner MM, Hoffman A, Radovcic J,
1007 Toussaint M, Kruszynski R, Menter C, Moggi-Cecchi J, Glasmacher UA, Kullmer O,
1008 Schrenk F, Stringer C, Hublin J-J. 2012. Variation in enamel thickness within the genus
1009 *Homo*. J Hum Evol 62:395-411.
1010 Spencer MA. 1998. Force production in the primate masticatory system: electromyographic
1011 tests of biomechanical hypotheses. J Hum Evol 34:25-54.
1012 Spencer MA. 1999. Constraints on masticatory system evolution in anthropoid primates. Am
1013 J Phys Anthropol 108:483-506.
1014 Spencer MA, Demes B. 1993. Biomechanical analysis of masticatory system configuration in
1015 Neandertals and Inuits. Am J Phys Anthropol 91:1-20.
1016 Spencer MA, Ungar PS. 2000. Craniofacial morphology, diet and incisor use in three native
1017 American populations. Inter J Osteoarchaeol 10:229-241.
1018 Spencer MA. 2003. Tooth-root form and function in platyrrhine seed-eaters. Am J Phys
1019 Anthropol 122:325-335.
1020 Strait DS, Grine FE. 2004. Inferring hominoid and early hominid phylogeny using craniodental
1021 characters: the role of fossil taxa. J Hum Evol 47:399-452.
1022 Strait DS, Grine FE, Moniz MA. 1997. A reappraisal of early hominid phylogeny. J Hum Evol
1023 32:17-82.
1024 Strait DS, Wang O, Dechow PC, Ross CF, Richmond BG, Spencer MA, Patel BA. 2005.
1025 Modeling elastic properties in finite element analysis: how much precision is needed to
1026 produce and accurate model? Anat Rec 283A:275-287.
1027 Strait DS, Richmond BG, M. A. Spencer, C. F. Ross, Dechow PC, Wood BW. 2007. Masticatory

biomechanics and its relevance to early hominid phylogeny: an examination of palatal thickness using finite-element analysis. J Hum Evol 52:585-599.

Strait DS, Weber GW, Neubauer S, Chalk J, Richmond BG, Lucas PW, Spencer MA, Schrein C, Dechow PC, Ross CF, Grosse IR, Wright BW, Constantino P, Wood BA, Lawn B, Hylander WL, Wang Q, Byron C, Slice DE, Smith AL. 2009. The feeding biomechanics and dietary ecology of *Australopithecus africanus*. Proc Natl Acad Sci USA 106:2124-2129.

Strait DS, Grosse IR, Dechow PC, Smith AL, Wang QW, Weber GW, Neubauer S, Slice DE, Chalk J, Richmond BG, Lucas PW, Spencer MA, Schrein C, Wright BW, Byron C, Ross CF. 2010. The structural rigidity of the cranium of *Australopithecus africanus*: implications for diet, dietary adaptations, and the allometry of feeding biomechanics. Anat Rec 298:583–593.

Strait DS, Constantino P, Lucas PW, Richmond BG, Spencer MA, Dechow PC, Ross CF, Grosse IR, Wright BW, Wood BA, Weber GW, Wang Q, Byron C, Slice DE, Chalk J, Smith AL, Smith LC, Wood S, Berthaume M, Benazzi S, Dzialo C, Tamvada K, Ledogar JA. 2013. Diet and dietary adaptations in early hominins: the hard food perspective. Am J Phys Anthropol 151:339-355.

Szwedowski TD, Fialkov F, Whyne CM. 2011. Sensitivity analysis of a validated subject-specific finite element model of the human craniofacial skeleton. Proc Inst Mech Eng H 225:58-67.

Taylor AB, Vinyard CJ. 2013. The relationships among jaw-muscle fiber architecture, jaw morphology, and feeding behavior in extant apes and modern humans. Am J Phys Anthrpol 151:120-134.

1051 Toro-Ibacache V, Zapata Muñoz V, O'Higgins P. 2015. The relationship between skull
1052 morphology, masticatory muscle force and cranial skeletal deformation during biting.
1053 Toro-Ibacache V, Fitton LC, Fagan MJ, O'Higgins P. 2015. Validity and sensitivity of a human
1054 cranial finite element model: implications for comparative studies of biting performance.
1055 Trinkaus E. 1983. Neanderthal postcrania and the adaptive shift to modern humans. In: The
1056 Mouseterian legacy: human biocultural change in the Upper Pleistocene. p 165-200.
1057 BAR.
1058 Trinkaus E. 1987. The Neandertal face: evolutionary and functional perspectives on a recent
1059 hominid face. J Hum Evol 16:429-443.
1060 Ungar P. 2012. Dental evidence for the reconstruction of diet in African early *Homo*. Curr
1061 Anthropol 53 S318-S329.
1062 Ungar PS, Grine FE, Teaford MF. 2006. Diet in early *Homo*: a review of the evidence and a
1063 new model of adaptive versatility. Ann Rev Anthropol 35:209-228.
1064 van Eijden TMGJ, Korfage JAM, Brugman P. 1997. Architecture of the human jaw-closing and
1065 jaw-opening muscles. Anat Rec 248:464-474.
1066 Vogel ER, van Woerden JT, Lucas PW, Atmoko SSU, van Schaik CP, Dominy NJ. 2008.
1067 Functional ecology and evolution of hominoid molar enamel thickness: *Pan troglodytes*
1068 *schweinfurthii* and *Pongo pygmaeus wurmbii*. J Hum evol 55:60-74.
1069 Walker AC. 1991. The origin of genus *Homo*. In: Osawa S, Honjo T, editors. Evolution of Life:
1070 Fossils, Molecules, and Culture. Tokyo: Springer-Verlag. p 379-389.
1071 Waltimo A, Nystram M, Kananen M. 1994. Bite force and dentofacial morphology in men with
1072 severe dental attrition. E J Oral Sci 102:92-96.
1073 Wang Q, Dechow PC. 2006. Elastic properties of external cortical bone in the craniofacial

skeleton of the rhesus monkey. Am J Phys Anthropol 131:402-415.

Wang Q, Strait DS, Dechow PC. 2006. A comparison of cortical elastic properties in the craniofacial skeletons of three primate species and its relevance to human evolution. J Hum Evol 51:375-382.

Wang Q, Wood SA, Grosse IR, Ross CF, Zapata U, Byron CD, Wright BW, Strait DS. 2012. The role of sutures in biomechanicanical dynamic simulation of a macaque cranial finite element model: implications for the evolution of craniofacial form. Anat Rec 295:278–288.

Waugh LM. 1937. Influence of diet on the jaws and face of the American Eskimo. J Amer Dental Assoc 24:1640-1647.

Weijs WA, Hillen B. 1984. Relationships between masticatory muscle cross-section and skull shape. J Dent Res 63:1154-1157.

Wood BA. 1992. Origin and early evolution of genus *Homo*. Nature 355:783-790.

Wood BA. 2009. “Where does the genus *Homo* begin, and how would we know?” The first humans: origins of the genus *Homo.* In: Grine FE, Fleagle JG, Leakey RE, editors. New York: Springer. p 17-28.

Wrangham RW. 2009. Catching fire: how cooking made us human. New York: Basic Books.

Wrangham RW, Jones JH, Laden G, Pilbeam D, Conklin-Brittain N. 1999. The raw and the stolen: cooking and the ecology of human origins. Curr Anthropol 40:567-594.

Wroe S, Ferrara TL, McHenry CR, Curnoe D, Chamoli U. 2010. The craniomandibular mechanics of being human. Proc R Soc Lond B Biol Sci 277:3579-3586.

Zink KD, Lieberman DE. 2016. Impact of meat and Lower Palaeolithic food processing

techniques on chewing in humans. Nature (Early View). doi:10.1038/nature16990.

Table 1(on next page)

Craniofacial landmarks used in the geometric morphometric analysis of human craniofacial shape.

Landmark	No.	Landmark	No.
Alare (R, L)	13, 40	Lingual canine margin (R, L)	124, 115
Alveolare	11	M1-M2 contact (R, L)	119, 128
Anterior nasal spine	10	M2-M3 contact (R, L)	120, 129
Anterior pterion (R, L)	24, 51	Malar root origin (R, L)	31, 58
Basion	67	Mid post-toral sulcus	6
Bregma	5	Midline anterior palatine	70
Canine-P3 contact (R, L)	116, 125	Mid-torus inferior (R, L)	21, 48
Center of mandibular fossa (R, L)	97, 103	Mid-torus superior (R, L)	22, 49
Dacryon (R, L)	16, 43	Nasion	8
Distal M3 (R, L)	121, 130	Opisthion	66
Frontomalare orbitale (R, L)	20, 47	Orbitale (R, L)	18, 45
Frontomalare temporale (R, L)	19, 46	P3-P4 contact (R, L)	117, 126
Frontosphenomalare (R, L)	23, 50	P4-M1 contact (R, L)	118, 127
Frontotemporale (R, L)	35, 62	Porion (R, L)	27, 54
Glabella	7	Postglenoid (R, L)	94, 100
Hormion	68	Rhinion	9
Incisivon	71	Root of zygomatic process (R, L)	32, 59
Inferior entoglenoid (R, L)	95, 101	Spheno-palatine suture (R, L)	108, 112
Inferior zygotemporal suture (R, L)	72, 78	Staphylion	69
Infraorbital foramen (R, L)	12, 39	Superior zygotemporal suture (R, L)	25, 52
Inion	1	Supraorbital notch (R, L)	17, 44
Jugale (R, L)	26, 53	Temporo-sphenoid suture (R, L)	109, 113
Lambda	3	Zygomaxillare (R, L)	14, 41
Lateral articular fossa (R, L)	96, 102	Zygoorbitale (R, L)	15, 42
Lateral prosthion (R, L)	114, 123		

Table 2(on next page)

Geographic distribution of human cranial specimens included in the analysis of craniofacial shape variation.

All specimens are housed at the American Museum of Natural History (AMNH).

Region/Population	N
Aboriginal Australian	9
Khoe-San, South Africa	3
China	6
East Africa	7
Grand Gulch, Utah	10
Greifenberg, Carinthia, Austria	6
Heidenheim, Germany	1
Kakoletri, Peloponnesus, Greece	1
Maori, Waitakeri, New Zealand	4
Mongolia	1
Point Hope, Alaska	12
Southeast Asia	12
Tarnapol, Galicia, Poland	2
Tasmanian	4
Tierra del Fuego, Argentina	3
West Africa	7

1

2

Table 3(on next page)

The 25 specimens most distant from the group centroid sorted by their distance from the group centroid.

Values in parentheses represent the distances expressed in units of mean distance. The bottom row represents an “average” representative of human cranial shape based on its close proximity to the group centroid. Specimens are coded here following American Museum of Natural History (AMNH) catalog numbers.

Specimen	Region/Population	Distance from centroid
VL/2463[1]	Khoe-San, South Africa	0.1011 (1.49)
VL/3878[1]	Greifenberg, Austria	0.0939 (1.38)
99/7889[1]	Malay Archipelago, SE Asia	0.0918 (1.35)
VL/3818	Greifenberg, Austria	0.0885 (1.31)
VL/269	Tasmanian	0.0881 (1.30)
VL/229	Kalmuk, Western Mongolia	0.0876 (1.29)
VL/408	Mhehe, East Africa	0.0871 (1.28)
99.1/511[1]	Point Hope, Alaska	0.0871 (1.28)
99/8155	Aboriginal Australian	0.0842 (1.24)
99/6562	Māori, New Zealand	0.0830 (1.22)
VL/271	Tasmanian	0.0824 (1.22)
VL/2470[1]	Khoe-San, South Africa	0.0788 (1.16)
VL/1902	Māori, New Zealand	0.0777 (1.15)
99.1/490	Point Hope, Alaska	0.0770 (1.14)
99/8165	Aboriginal Australian	0.0767 (1.13)
VL/272	Tasmanian	0.0750 (1.11)
VL3619	Greifenberg, Austria	0.0745 (1.10)
99/7333	Grand Gulch, Utah	0.0741 (1.09)
99/8177	Aboriginal Australian	0.0740 (1.09)
VL/2267	Kakoletri, Greece	0.0733 (1.08)
VL/1729	Tientsin, China	0.0728 (1.07)
VL/1602[1]	Ashanti, West Africa	0.0727 (1.07)
VL/274	Tasmanian	0.0721 (1.06)
VL/2389	Ashanti, West Africa	0.0721 (1.06)
99/8171	Aboriginal Australian	0.0720 (1.06)
99/7365[1]	Grand Gulch, Utah	0.0496 (0.73)

[1] Specimens selected to be modeled using FEA.

Table 4(on next page)

Pairwise distances between the 6 human cranial specimens selected for use in finite element analysis.

Values in parentheses represent the distances expressed in units of mean pairwise distance.

Specimens are coded here following American Museum of Natural History (AMNH) catalog numbers.

	VL/2463	VL/3878	99/7889	99.1/511	VL/2470	VL/1602
VL/2463		0.1634 (1.70)[1]	0.0938 (0.97)	0.1534 (1.59)[1]	0.1083 (1.12)	0.1145 (1.19)
VL/3878			0.1469 (1.52)	0.1304 (1.35)	0.1230 (1.28)	0.1385 (1.44)
99/7889				0.1526 (1.58)[1]	0.1178 (1.22)	0.1029 (1.09)
99.1/511					0.1330 (1.38)	0.1256 (1.30)
VL/2470						0.1049 (1.09)
VL/1602						

[1]These represent the greatest pairwise distances in the final sample.

Table 5(on next page)

Muscle force scaling for the ALL-HUM and CHIMPED models of modern human crania.

Models are ordered from smallest to largest volume (and applied force). AT = anterior temporalis, SM = superficial masseter, DM = deep masseter, MP = medial pterygoid.

Variant	Model	Volume	Volume$^{2/3}$	AT	SM	DM	MP
ALL-HUM	KSAN2	331466	4789.53	128.41	105.15	53.29	108.64
	MALP	364129	5099.22	136.72	111.95	56.73	115.67
	KSAN2	433331	5726.38	153.53	125.72	63.71	129.89
	WAFR	475555	6092.57	163.35	133.75	67.79	138.20
	BERG	489588	6211.84	166.55	136.37	69.11	140.90
	GRGL	557223	6771.52	181.55	148.66	75.34	153.60
	TIGA	655320	7544.59	202.28	165.63	83.94	171.14
CHIMPED	KSAN2	331466	4789.53	556.13	572.02	85.07	189.02
	MALP	364129	5099.22	592.09	609.00	90.57	201.24
	KSAN2	433331	5726.38	664.91	683.90	101.71	225.99
	WAFR	475555	6092.57	707.43	727.64	108.22	240.44
	BERG	489588	6211.84	721.28	741.88	110.34	245.15
	GRGL	557223	6771.52	786.26	808.73	120.28	267.24
	TIGA	655320	7544.59	876.02	901.05	134.01	297.74

1

Table 6(on next page)

Results of *in vitro* validation analysis.

Average values and standard deviations for maximum (MaxPrin) and minimum (MinPrin) principal strain magnitudes recorded during three *in vitro* loading trials on the left P^3 biting , the results of a specimen-specific *in silico* (FEA) loading analysis, and an estimate of the error in the FEA, where “error” is represented by the difference between *in vitro* (observed) and *in silico* (expected) results, divided by the expected results. See Fig. S3 – Fig. S7 for site locations. Units are in microstrain (με).

Site	Exp.	MaxPrin	MinPrin	Site	Exp.	MaxPrin	MinPrin
1.	***In vitro***	15.00 (4.36)	-10.33 (2.08)	**8.**	***In vitro***	42.33 (2.08)	-109.67 (3.06)
	In silico	14	-15		***In silico***	37	-105
	Error	6.67%	45.16%		**Error**	12.60%	4.26%
2.	***In vitro***	13.00 (1.00)	-11.67 (0.58)	**9.**	***In vitro***	7.67 (0.58)	-2.67 (2.08)
	In silico	10	-10		***In silico***	8	-4
	Error	23.08%	14.29%		**Error**	4.35%	50.00%
3.	***In vitro***	3.33 (0.58)	-5.00 (1.00)	**10.**	***In vitro***	45.33 (2.08)	-22.33 (1.15)
	In silico	6	-7		***In silico***	23	-20
	Error	80.00%	40.00%		**Error**	49.26%	10.45%
4.	***In vitro***	30.67 (1.15)	-36.00 (0.00)	**11.**	***In vitro***	23.67 (0.58)	-10.67 (3.06)
	In silico	29	-34		***In silico***	22	-13
	Error	5.43%	5.56%		**Error**	7.04%	21.88%
5.	***In vitro***	15.00 (2.00)	-14.67 (1.53)	**12.**	***In vitro***	108.00 (2.65)	-281.67 (8.33)
	In silico	19	-12		***In silico***	115	-238
	Error	26.67%	18.18%		**Error**	6.48%	15.50%
6.	***In vitro***	11.67 (0.58)	-7.33 (0.58)	**13.**	***In vitro***	38.67 (1.15)	-22.00 (1.00)
	In silico	11	-10		***In silico***	39	-17
	Error	5.71%	36.36%		**Error**	0.86%	22.73%
7.	***In vitro***	42.33 (1.53)	-23.33 (2.25)	**14.**	***In vitro***	27.67 (2.08)	-42.33 (3.01)
	In silico	42	-17		***In silico***	38	-25
	Error	0.79%	27.14%		**Error**	37.35%	40.94%

1

2

Table 7 (on next page)

Variation in strain and strain energy density in the ALL-HUM models.

Coefficients of variation for maximum principal strain (MaxPrin), minimum principal strain (MinPrin), shear strain (Shear), von Mises strain, and strain energy density (SED) at the 14 locations examined during premolar (P^3) and molar (M^2) biting in the ALL-HUM models of modern human crania. Site numbers follow Figure 4.

Site	Bite	MaxPrin	MinPrin	Shear	von Mises	SED
1	P^3	56.01	34.39	28.49	27.88	59.08
	M^2	43.20	28.62	20.78	22.82	50.07
2	P^3	28.35	41.61	30.51	29.27	78.82
	M^2	27.61	44.20	29.50	29.04	60.38
3	P^3	23.83	26.53	22.94	22.97	52.39
	M^2	25.16	24.29	24.66	24.16	49.48
4	P^3	15.30	21.39	14.75	14.28	27.78
	M^2	34.43	22.83	22.73	21.46	36.89
5	P^3	14.32	13.06	12.77	13.24	26.98
	M^2	12.50	14.22	11.70	12.06	24.53
6	P^3	21.74	12.21	11.77	11.89	23.52
	M^2	17.43	13.56	11.13	12.05	25.11
7	P^3	12.53	8.26	8.09	7.93	15.97
	M^2	11.27	6.05	5.78	5.32	11.98
8	P^3	19.73	2.58	13.87	12.50	25.96
	M^2	20.48	12.04	12.62	11.88	23.36
9	P^3	20.78	21.84	18.18	19.30	39.77
	M^2	12.59	9.28	8.23	8.66	19.36
10	P^3	11.70	33.05	12.32	11.72	21.21
	M^2	35.51	22.16	25.60	25.86	50.44
11	P^3	24.44	37.84	24.15	21.83	36.54
	M^2	25.53	43.20	28.88	26.73	52.39
12	P^3	51.04	35.54	39.39	37.44	64.43
	M^2	52.66	34.33	41.78	40.46	76.44
13	P^3	28.41	34.42	26.48	25.60	51.87
	M^2	14.11	20.80	14.37	13.50	28.05
14	P^3	35.54	22.56	31.16	31.33	68.31
	M^2	39.93	26.73	35.19	35.33	80.97

1

2

3

Table 8(on next page)

Variation in von Mises strain magnitudes: Human vs. Chimpanzee.

Comparisons of the coefficients of variation (CVs) for von Mises strain recorded in the CHIMPED human models and the chimpanzee results from Smith et al. (2015b) at each of the 14 craniofacial sites examined. Results of Fligner-Killeen tests for equal CVs between the species are also presented ($\alpha=0.05$). Comparisons that yielded significant results are shown in bold typeface.

Site		P^3	M^2	Site		P^3	M^2
1	CV - Human	29.04	22.68	**8**	CV - Humans	10.14	12.27
	CV - Chimp	25.91	23.63		CV - Chimps	16.54	25.58
	p (same CV)	0.065	0.141		p (same CV)	0.143	0.130
2	CV - Humans	24.34	23.05	**9**	CV - Humans	14.12	8.03
	CV - Chimps	46.61	47.07		CV - Chimps	25.7	23.58
	p (same CV)	0.122	0.050		p (same CV)	0.069	0.052
3	CV - Humans	19.71	17.75	**10**	CV - Humans	8.8	15.46
	CV - Chimps	19.81	20.10		CV - Chimps	17.36	15.30
	p (same CV)	0.386	0.369		p (same CV)	**0.039**	0.290
4	CV - Humans	13.51	21.12	**11**	CV - Humans	10.6	14.34
	CV - Chimps	29.98	33.20		CV - Chimps	27.76	28.11
	p (same CV)	0.176	0.359		p (same CV)	0.056	0.100
5	CV - Humans	12.89	11.50	**12**	CV - Humans	38.05	38.76
	CV - Chimps	27.56	29.40		CV - Chimps	28.23	43.35
	p (same CV)	0.156	0.060		p (same CV)	0.147	0.396
6	CV - Humans	18.15	16.51	**13**	CV - Humans	24.54	10.39
	CV - Chimps	64.99	66.99		CV - Chimps	17.95	17.52
	p (same CV)	**0.022**	**0.022**		p (same CV)	0.157	0.207
7	CV - Humans	11.96	12.07	**14**	CV - Humans	22.78	23.11
	CV - Chimps	55.83	56.63		CV - Chimps	51.99	55.84
	p (same CV)	**0.022**	**0.022**		p (same CV)	0.222	0.166

1

2

Table 9(on next page)

Bite force production, biting efficiency, and joint reaction forces in the ALL-HUM model variants of human crania.

Bite force (BF), mechanical advantage (MA), working-side TMJ reaction force (RF-WS), and balancing-side TMJ reaction force (RF-BS) for premolar and molar biting. Five of seven ALL-HUM models generated distractive (tensile) reaction forces during molar loading. Therefore, balancing side muscle forces were iteratively reduced by 5% and re-run until distractive forces were eliminated. Bite and TMJ reaction forces are in Newtons (N).

Model	Muscle Force	Premolar Bite				Molar Bite			
		BF	MA	RF-WS	RF-BS	BF	MA	RF-WS	RF-BS
GRGL	1118	441	0.39	167.42	349.25	658	0.59	-11.74	329.79
GRGL[1]	1090					642	0.59	-1.37	311.18
GRGL[2]	1062					625	0.59	8.98	292.58
BERG	1026	439	0.43	147.72	281.55	663	0.65	-6.98	249.09
BERG[1]	1000					647	0.65	1.29	234.72
KSAN1	946	378	0.40	121.76	295.69	538	0.57	-17.49	280.57
KSAN1[2]	898					511	0.57	0.07	249.74
KSAN2	791	333	0.42	106.83	240.30	496	0.63	-18.86	222.80
KSAN2[2]	751					471	0.63	-4.26	197.88
KSAN2[3]	732					459	0.63	3.04	185.41
MALP	842	344	0.41	131.09	277.66	537	0.64	-19.85	274.49
MALP[2]	800					510	0.64	-0.99	242.97
TIGA	1246	507	0.41	187.96	373.24	756	0.61	13.68	336.84
WAFR	1006	341	0.34	149.36	298.77	529	0.53	12.64	273.79

[1]Model re-run using muscle forces reduced by 5% on the balancing side.
[2]Model re-run using muscle forces reduced by 10% on the balancing side.
[3]Model re-run using muscle forces reduced by 15% on the balancing side.

Table 10(on next page)

Von Mises strain magnitudes: Human vs. Chimpanzee.

Results of pairwise comparisons (Mann-Whitney *U*-test) of von Mises strain magnitudes at the 14 locations examined between CHIMPED variants of human FEMs and data on chimpanzees from Smith et al. (2015b). Because of small sample sizes, the ‘‘exact’’ variant of p is reported (Mundry and Fischer, 1998). Comparisons that yielded significant results following Holm-Bonferroni correction are shown in bold typeface. When significant, humans were found to exhibit the higher average value, with the exception of locations 13 and 14.

Site	Bite	U	z	Exact p
1. Dorsal interorbital	Premolar	9	-1.65	0.0967
	Molar	10	-1.50	0.1265
2. Working dorsal orbital	Premolar	0	-2.93	**0.0012**
	Molar	0	-2.93	**0.0012**
3. Balancing dorsal orbital	Premolar	4	-2.36	0.0140[1]
	Molar	7	-1.93	0.0513
4. Working postorbital bar	Premolar	0	-2.93	**0.0012**
	Molar	1	-2.79	**0.0023**
5. Balancing postorbital bar	Premolar	0	-2.93	**0.0012**
	Molar	0	-2.93	**0.0012**
6. Working zygomatic arch	Premolar	14	-0.93	0.3660
	Molar	14	-0.93	0.3660
7. Balancing zygomatic arch	Premolar	14	-0.93	0.3660
	Molar	14	-0.93	0.3660
8. Working zygomatic root	Premolar	0	-2.93	**0.0012**
	Molar	0	-2.93	**0.0012**
9. Balancing zygo root	Premolar	18	-0.36	0.7308
	Molar	11	-1.36	0.1807
10. Working infraorbital	Premolar	2	-2.64	**0.0047**
	Molar	7.5	-1.86	0.0565
11. Balancing infraorbital	Premolar	6	-2.07	0.0350[1]
	Molar	12	-1.21	0.2343
12. Working nasal margin	Premolar	0	-2.93	**0.0012**
	Molar	1	-2.79	**0.0023**
13. Working zygomatic body	Premolar	0	-2.93	**0.0012**
	Molar	1	-2.79	**0.0023**
14. Balancing zygomatic body	Premolar	0.5	-2.86	**0.0017**
	Molar	1	-2.79	**0.0023**

[1]Result is significant at $p \leq 0.05$.

Table 11(on next page)

Bite force production, biting efficiency, and joint reaction forces in the CHIMPED model variants of human crania.

Bite force (BF), mechanical advantage (MA), working-side temporomandibular joint reaction force (RF-WS), and balancing-side temporomandibular joint reaction force (RF-BS) for premolar and molar biting. All seven CHIMPED models generated highly distractive (tensile) reaction forces during molar loading that would have increased the chances of joint dislocation and/or injury. Therefore, balancing side muscle forces were iteratively reduced by 5% and re-run until distractive forces were eliminated. Bite and TMJ reaction forces are in Newtons (N).

Model	Muscle Force	Premolar Bite				Molar Bite			
		BF	MA	RF-WS	RF-BS	BF	MA	RF-WS	RF-BS
GRGL	3965	1724	0.43	499.82	1189.57	2570	0.65	-208.16	1113.51
GRGL[1]	3569					2316	0.65	-31.26	841.64
GRGL[2]	3469					2252	0.65	12.96	773.68
BERG	3637	1720	0.47	405.08	935.03	2599	0.71	-185.65	819.81
BERG[2]	3183					2277	0.71	-6.72	560.17
BERG[3]	3092					2213	0.71	29.07	508.24
KSAN1	3353	1462	0.44	343.26	1030.37	2080	0.62	-187.95	975.38
KSAN1[2]	2934					1822	0.62	-0.30	687.33
KSAN1[3]	2850					1771	0.62	37.23	629.72
KSAN2	2804	1272	0.45	311.70	821.79	1895	0.68	-163.75	757.22
KSAN2[2]	2454					1658	0.68	-11.46	529.80
KSAN2[3]	2384					1610	0.68	18.99	484.32
MALP	2986	1358	0.45	384.41	966.38	2118	0.71	-203.31	963.66
MALP[2]	2613					1851	0.71	-2.01	667.11
MALP[3]	2538					1797	0.71	38.25	607.81
TIGA	4418	1941	0.44	564.13	1288.46	2896	0.66	-107.59	1143.16
TIGA[4]	4197					2750	0.66	-13.27	997.33
TIGA[5]	4086					2678	0.66	33.89	924.42
WAFR	3567	1383	0.39	489.34	1103.22	2146	0.60	-61.09	1006.50
WAFR[6]	3478					2091	0.60	-24.01	946.69
WAFR[4]	3389					2036	0.60	13.07	886.88

[1]Model re-run using muscle forces reduced by 20% on the balancing side.
[2]Model re-run using muscle forces reduced by 25% on the balancing side.
[3]Model re-run using muscle forces reduced by 30% on the balancing side.
[4]Model re-run using muscle forces reduced by 10% on the balancing side.
[5]Model re-run using muscle forces reduced by 15% on the balancing side.
[6]Model re-run using muscle forces reduced by 5% on the balancing side.

1

The constrained lever model of jaw biomechanics.

During biting, the bite point (b) and the temporomandibular joints on the working side (ws) and balancing side (bs) form a “triangle of support” that changes shape when biting on different teeth. During a premolar bite (**A**), the resultant vector of the jaw adductor muscles (v) passes through the triangle, producing compression (green circles) at all three points. However, during some molar bites (**B**), the vector falls outside the triangle when the muscles are being recruited equally on both sides of the head, producing compression at the bite point and bs joint, but distraction (red circle) at the ws joint. The recruitment of the balancing side muscles must be lessened in order to eliminate this distraction, thereby causing the vector to shift its position towards the working side and back into the triangle (yellow arrow).

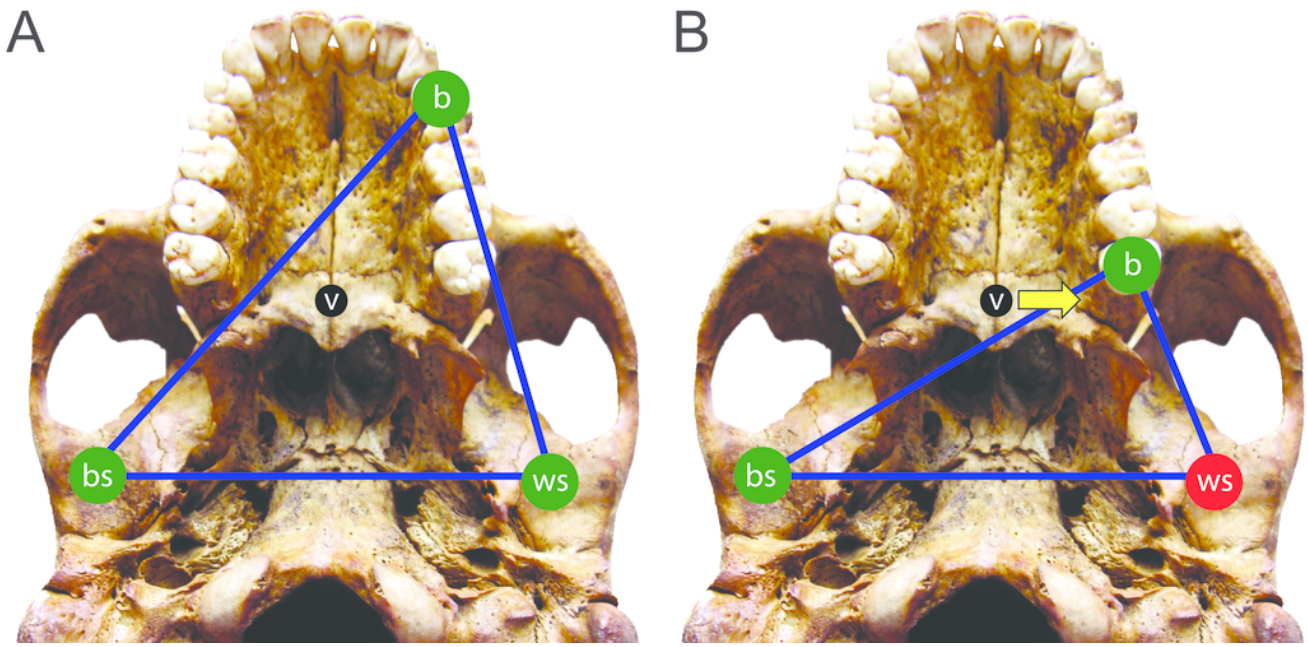

2

Principal component analysis (PCA) of human craniofacial shape variation.

Panels show (**A**) PC1 by PC2, (**B**) PC1 by PC3, and (**C**) wireframes illustrating craniofacial shape change associated with the first three principal components in right lateral, superior, and frontal views. The left and right columns of wireframes represent the negative and positive ends of each component, respectively, scaled to their respective axes. The 10 unique landmarks with the highest loadings are highlighted in red for each component on the midline and right side. A single ellipse was used to circle multiple landmarks if they were located close together. Shape differences toward the positive end of PC 1 include: a vertically shorter face with a more projecting brow ridge, a longer and more projecting palate, a more vertical frontal bone that is narrower at pterion, a vault that is expanded posteriorly, and a lower temporal line at stephanion. Shape differences toward the positive end of PC 2 include: a longer cranium with a wider frontal bone, a vault that is angled more postero-inferiorly, wider orbits and a superiorly shifted nasal aperture, and an antero-posteriorly shorter temporal bone. Shape differences toward the positive end of PC 3 include: higher temporal lines at stephanion, a shorter and more orthognathic subnasal region with a less projecting palate, a more inferiorly positioned temporomandibular joint, and a more inferiorly positioned midline cranial base.

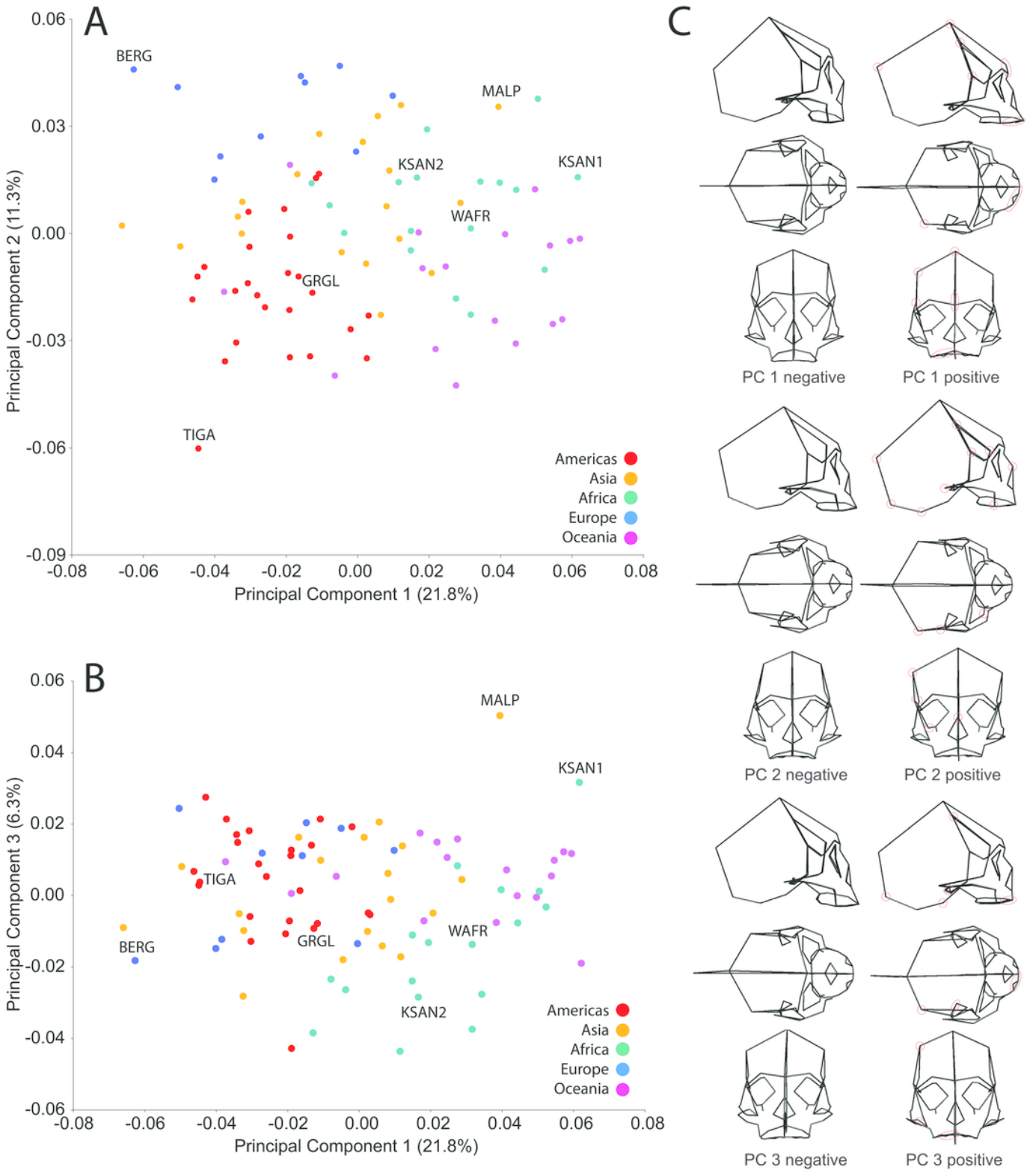
A
BERG
MALP
KSAN2
KSAN1
WAFR
GRGL
TIGA
Americas
Asia
Africa
Europe
Oceania
Principal Component 2 (11.3%)
Principal Component 1 (21.8%)
0.06
0.03
0.00
-0.03
-0.06
-0.09
-0.08
-0.06
-0.04
-0.02
0.00
0.02
0.04
0.06
0.08
B
MALP
KSAN1
TIGA
BERG
GRGL
WAFR
KSAN2
Americas
Asia
Africa
Europe
Oceania
Principal Component 3 (6.3%)
Principal Component 1 (21.8%)
0.06
0.04
0.02
0.00
-0.02
-0.04
-0.06
-0.08
-0.06
-0.04
-0.02
0.00
0.02
0.04
0.06
0.08
C
PC 1 negative
PC 1 positive
PC 2 negative
PC 2 positive
PC 3 negative
PC 3 positive

3

Human models analyzed in the current study.

Models include one “average” cranium, GRGL (**A**), and six “extreme” specimens that differ notably in shape, BERG (**B**), KSAN1 (**C**), KSAN2 (**D**), MALP (**E**), TIGA (**F**), and WAFR (**G**).

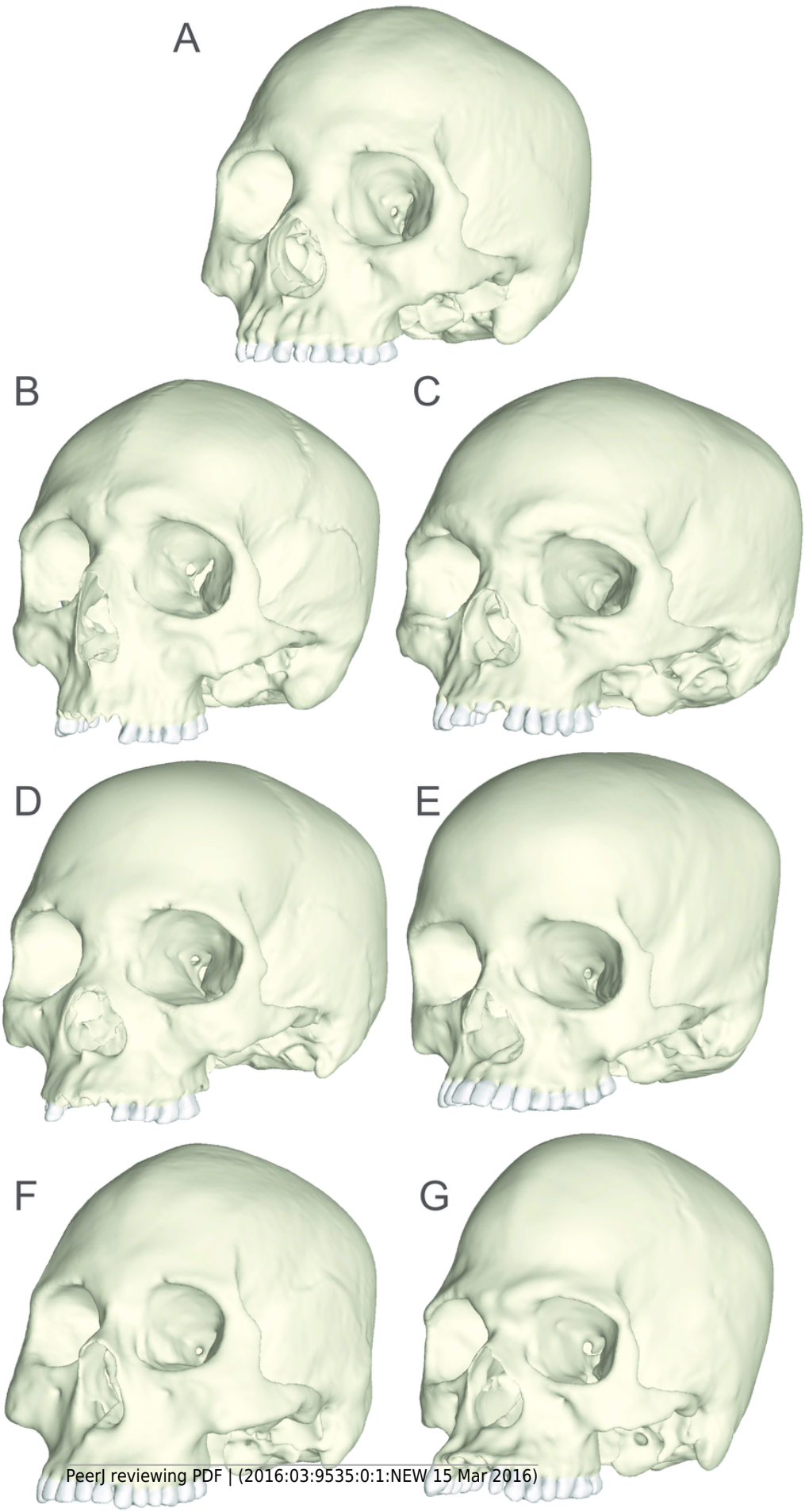
A
B
C
D
E
F
G

4

Key to locations where strains were sampled in finite element models.

Strain data were collected from ALL-HUM and CHIMPED variants of human FEMs from 14 craniofacial sites, following Smith et al. (2015a,b).

1	Dorsal Interorbital
2	Working Dorsal Orbital
3	Balancing Dorsal Orbital
4	Working Postorbital Bar
5	Balancing Postorbital Bar
6	Working Zygomatic Arch
7	Balancing Zygomatic Arch
8	Working Zygomatic Root
9	Balancing Zygomatic Root
10	Working Infraorbital
11	Balancing Infraorbital
12	Working Nasal Margin
13	Working Zygomatic Body
14	Balancing Zygomatic Body

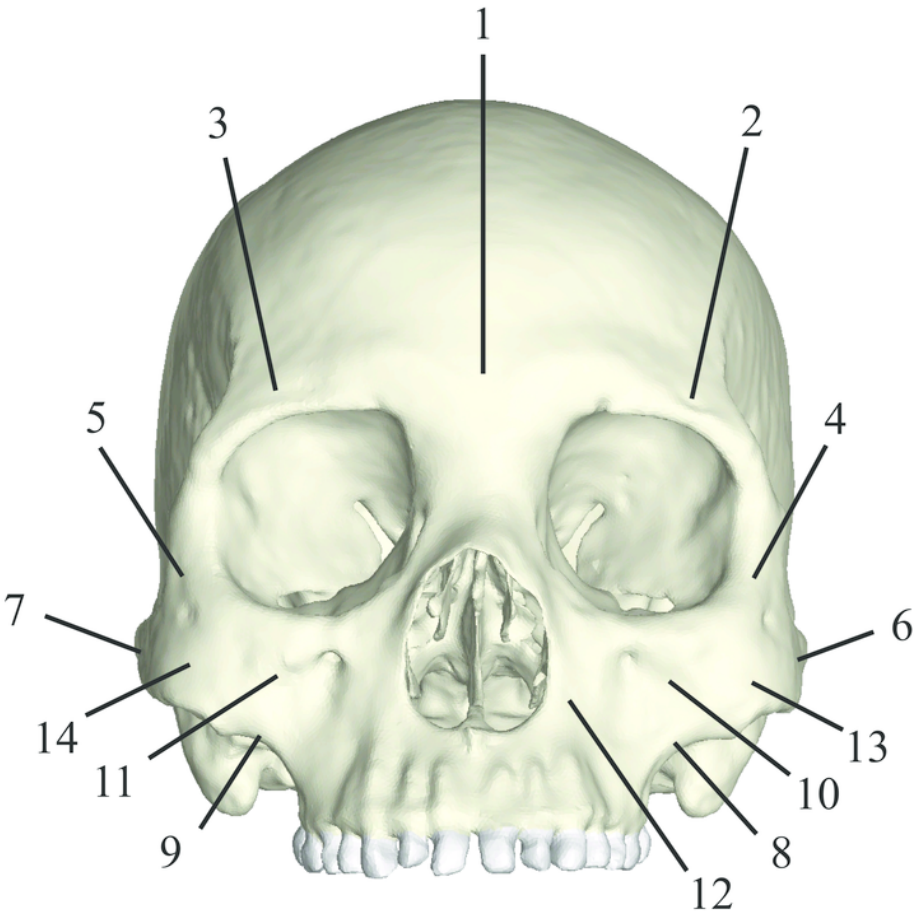

5

Strain and SED generated by the ALL-HUM models.

Box-and-whisker plots show the minimum, first quartile, median, third quartile, and maximum for strain and SED magnitudes (y-axis) generated by the ALL-HUM models at the 14 sampled locations (x-axis) during premolar (P^3) and molar (M^2) biting. Site numbers follow Fig. 4.

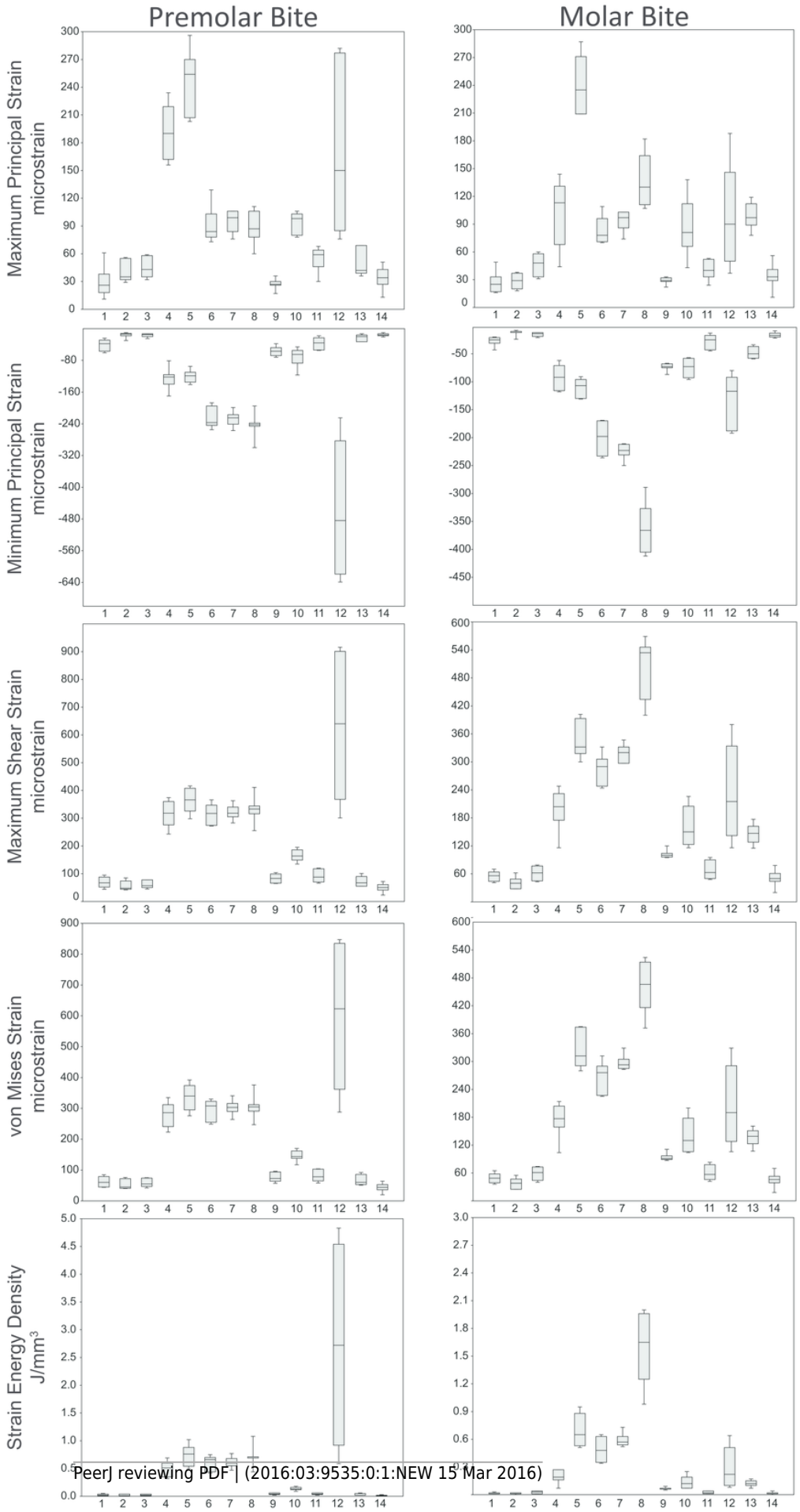
Premolar Bite
Molar Bite
Maximum Principal Strain microstrain
Minimum Principal Strain microstrain
Maximum Shear Strain microstrain
von Mises Strain microstrain
Strain Energy Density J/mm3

6

Strain mode in the ALL-HUM models.

Distribution of strain mode (log of ratio of maximum to minimum principal strain, y-axis) plotted by location (x-axis) in the ALL-HUM models. Plots show (**A**) premolar (P^3) and (**B**) molar (M^2) biting. Logging the data listed in Tables S2 and S3 centers strain mode data around zero. Values above zero indicate mainly tension, while values below zero indicate mainly compression. Site numbers follow Fig. 4.

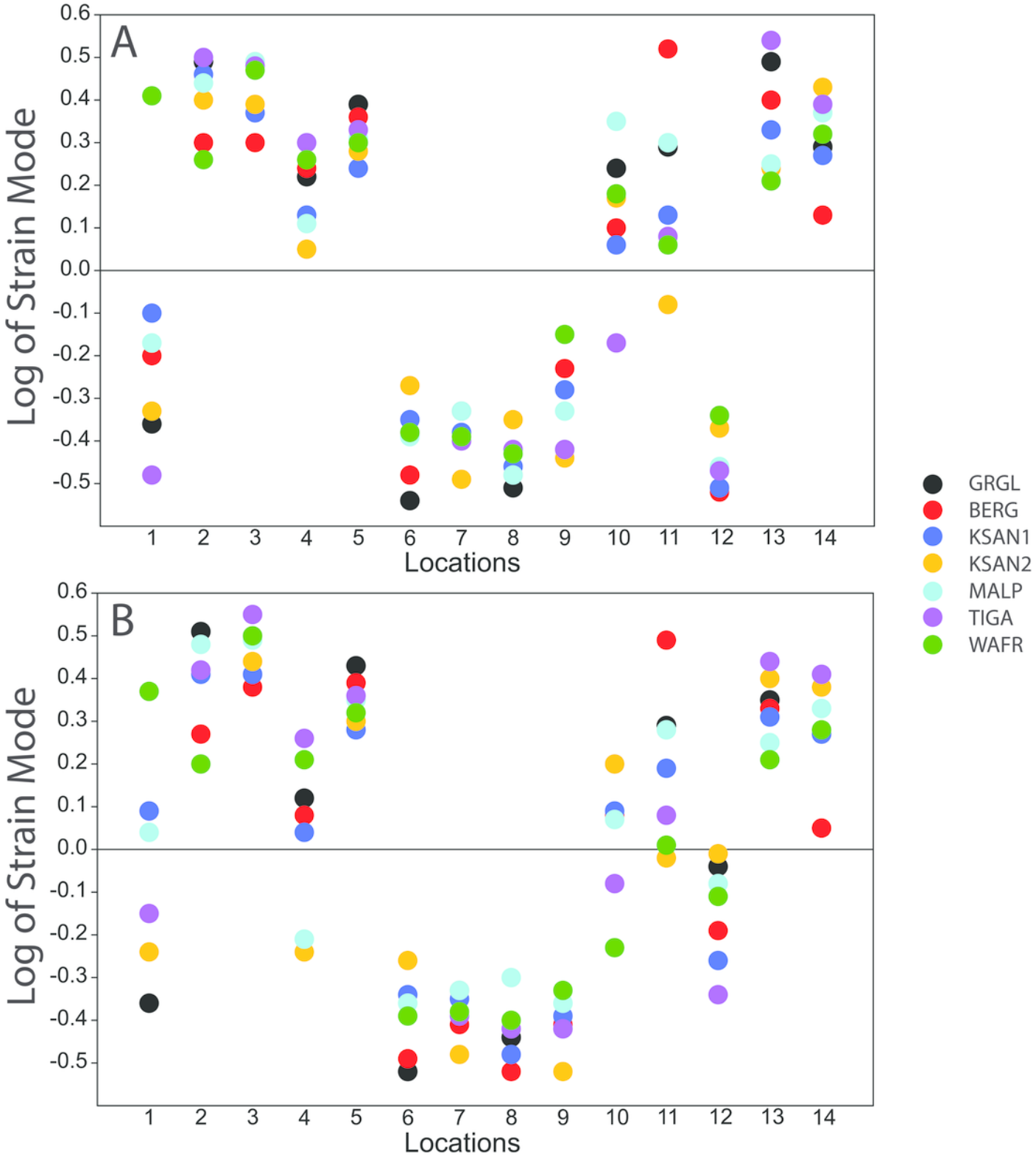
A
B
Log of Strain Mode
Locations
0.6
0.5
0.4
0.3
0.2
0.1
0.0
-0.1
-0.2
-0.3
-0.4
-0.5
1
2
3
4
5
6
7
8
9
10
11
12
13
14
GRGL
BERG
KSAN1
KSAN2
MALP
TIGA
WAFR

7

Strain distributions in the ALL-HUM models: P^3 biting.

Color maps of strain distributions in the ALL-HUM variants of “extreme” and “average” modern human cranial FEMs during premolar (P^3) biting. Scales are set to range from -150 – 150 με for both maximum principal strain (MaxPrin) and minimum principal strain (MinPrin), from 0 – 300 με for both maximum shear strain (Shear) and von Mises strain (von Mises), and from 0 – 0.5 J/mm^3 for strain energy density (SED). White regions exceed scale. Models are shown at the same height.

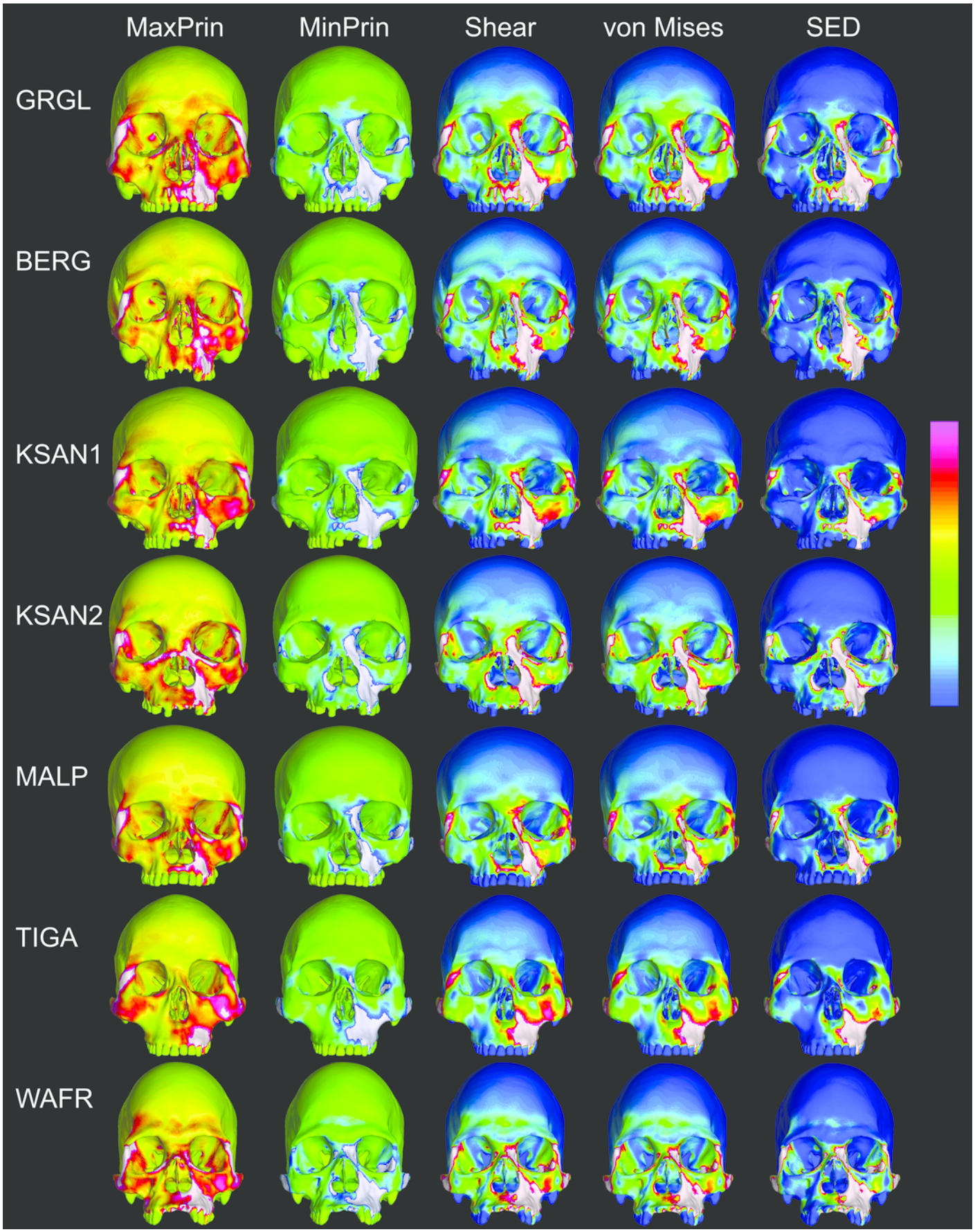
MaxPrin
MinPrin
Shear
von Mises
SED
GRGL
BERG
KSAN1
KSAN2
MALP
TIGA
WAFR

8

Strain distributions in the ALL-HUM models: M^2 biting.

Color maps of strain distributions in the ALL-HUM variants of “extreme” and “average” modern human cranial FEMs during molar (M^2) biting. Scales are set to range from -150 – 150 με for both maximum principal strain (MaxPrin) and minimum principal strain (MinPrin), from 0 – 300 με for both maximum shear strain (Shear) and von Mises strain (von Mises), and from 0 – 0.5 J/mm^3 for strain energy density (SED). White regions exceed scale. Models are shown at the same height.

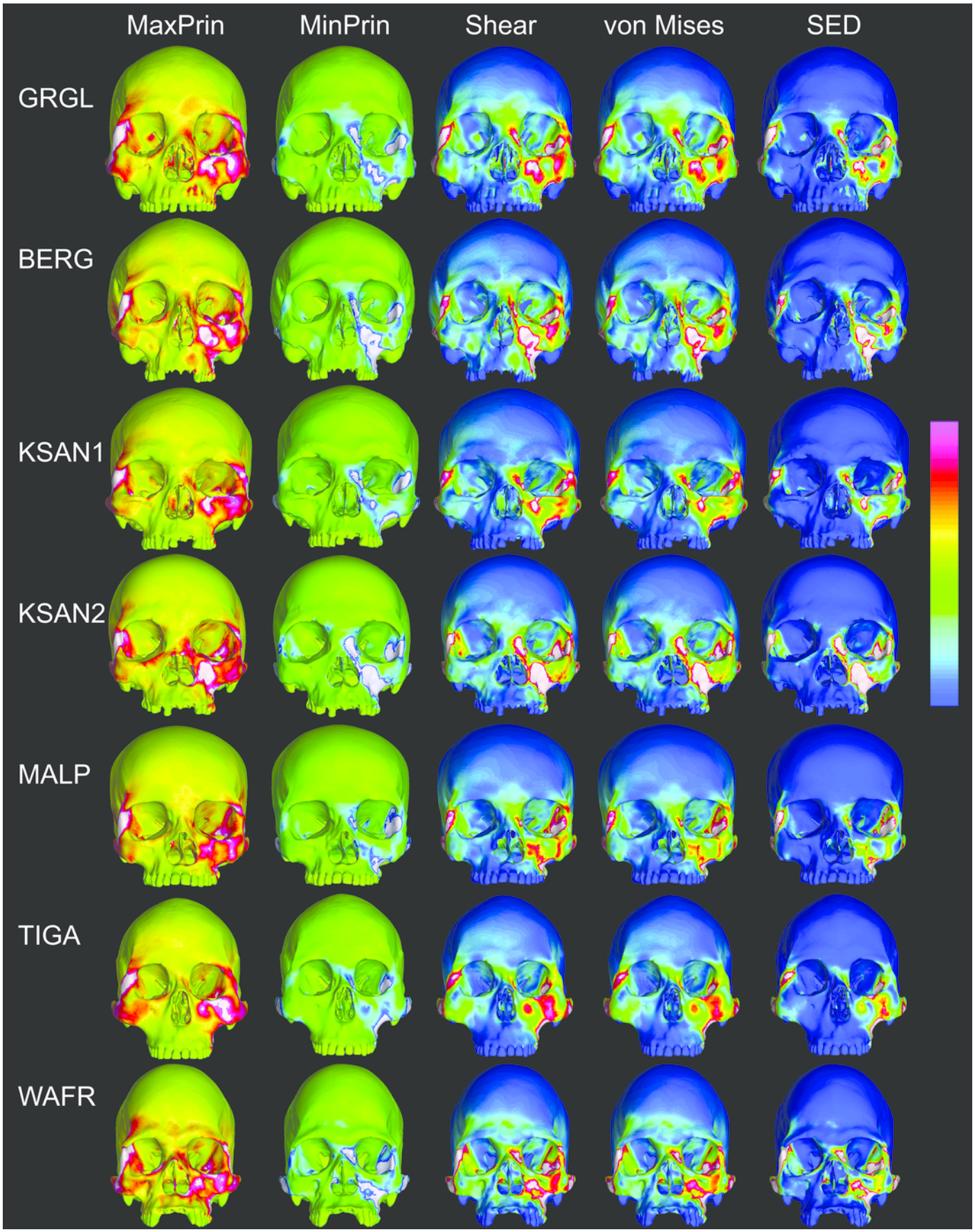
MaxPrin
MinPrin
Shear
von Mises
SED
GRGL
BERG
KSAN1
KSAN2
MALP
TIGA
WAFR

9

Relative strain distributions.

Color maps of “relative” maximum (MaxPrin) and minimum (MinPrin) principal strains in the CHIMPED model variants during premolar (P^3) and molar (M^2) biting. The scales range from -$\bar{x}$ to $\bar{x}$, where $\bar{x}$ differs in each image as follows: P^3, MaxPrin/MinPrin: GRGL, 612/644; BERG, 500/534; KSAN1, 508/603; KSAN2, 593/724; MALP, 520/610; TIGA, 455/498; WAFR, 672/742; M^2, MaxPrin/MinPrin: GRGL, 505/546; BERG, 468/525; KSAN1, 441/473; KSAN2, 505/546; MALP, 433/458; TIGA, 419/420; WAFR, 530/553. White regions exceed scale.

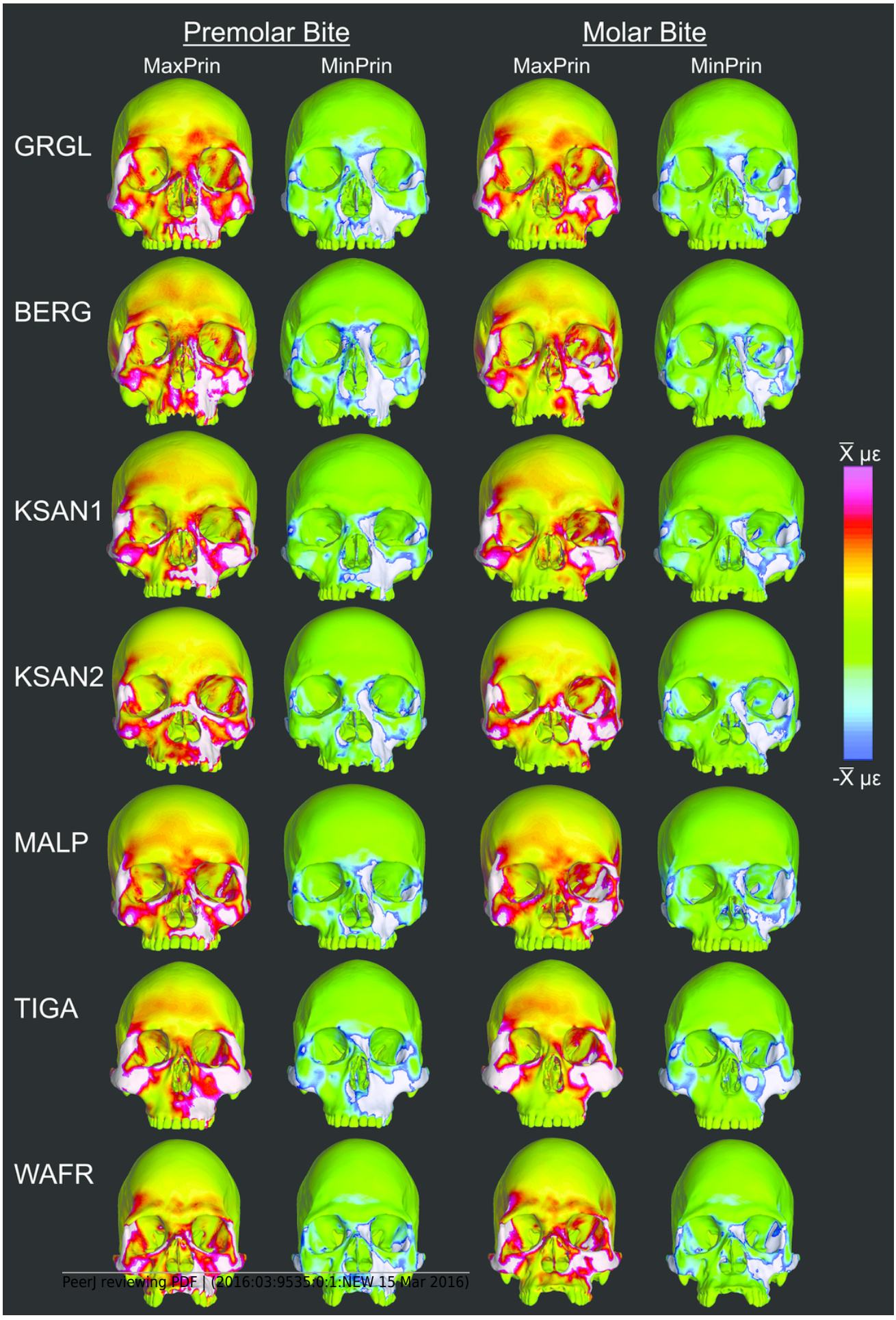
Premolar Bite
Molar Bite
MaxPrin
MinPrin
MaxPrin
MinPrin
GRGL
BERG
KSAN1
KSAN2
MALP
TIGA
WAFR
X̄ με
-X̄ με

10

Line plots of von Mises microstrain generated during simulated biting in finite element models of humans and chimpanzees.

Strain data correspond to (**A**) left premolar (P^3) and (**B**) left molar (M^2) biting, recorded from 14 homologous locations in the CHIMPED variants of “extreme” and “average” modern human cranial FEMs. The gray region brackets the range of variation observed for chimpanzees by Smith et al. (2015b).

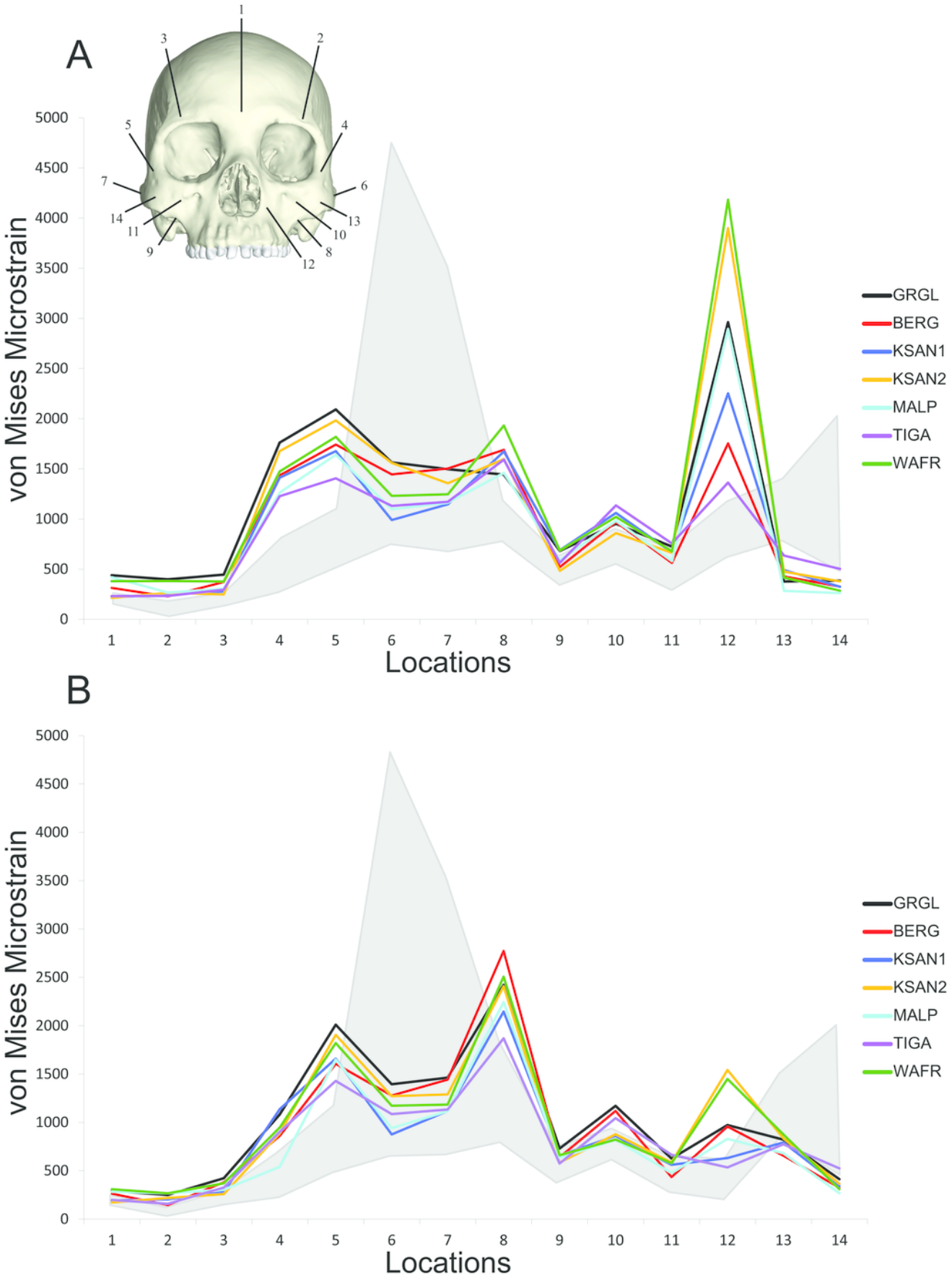
A
1
2
3
4
5
6
7
8
9
10
11
12
13
14
5000
4500
4000
3500
3000
2500
2000
1500
1000
500
0
von Mises Microstrain
1
2
3
4
5
6
7
8
9
10
11
12
13
14
Locations
GRGL
BERG
KSAN1
KSAN2
MALP
TIGA
WAFR
B
5000
4500
4000
3500
3000
2500
2000
1500
1000
500
0
von Mises Microstrain
1
2
3
4
5
6
7
8
9
10
11
12
13
14
Locations
GRGL
BERG
KSAN1
KSAN2
MALP
TIGA
WAFR

11

Biting efficiency: humans vs. chimpanzees.

Box-and-whisker plots show the minimum, first quartile, median, third quartile, and maximum biting efficiency, as quantified using the mechanical advantage (MA), in the CHIMPED variants of human cranial FEMs vs. chimpanzees at (**A**) premolar (P^3) and (**B**) molar (M^2) bite points. Chimpanzee data is from Smith et al. (2015b).